Journal of Medicinal Chemistry

Article

Antimalarial Inhibitors Targeting Serine Hydroxymethyltransferase (SHMT) with *In Vivo* Efficacy and Analysis of their Binding Mode Based on X-ray Cocrystal Structures

Geoffrey Schwertz, Matthias C. Witschel, Matthias Rottmann, Roger Bonnert, Ubolsree Leartsakulpanich, Penchit Chitnumsub, Aritsara Jaruwat, Wanwipa Ittarat, Anja Schäfer, Raphael A. Aponte, Susan A. Charman, Karen L. White, Abhijit Kundu, Surajit Sadhukhan, Mel Lloyd, Gail M. Freiberg, Myron Srikumaran, Marc Siggel, Adrian Zwyssig, Pimchai Chaiyen, and François Diederich

J. Med. Chem., **Just Accepted Manuscript** • Publication Date (Web): 24 May 2017

ACS Publications

Journal of Medicinal Chemistry is published by the American Chemical Society. 1155 Sixteenth Street N.W., Washington, DC 20036

Antimalarial Inhibitors Targeting Serine Hydroxymethyltransferase (SHMT) with *In Vivo* Efficacy and Analysis of their Binding Mode Based on X-ray Cocrystal Structures

Geoffrey Schwertz[†], Matthias C. Witschel[‡], Matthias Rottmann[§,ø], Roger Bonnert[||], Ubolsree Leartsakulpanich[⊥], Penchit Chitnumsub[⊥], Aritsara Jaruwat[⊥], Wanwipa Ittarat[⊥], Anja Schäfer[§,ø], Raphael A. Aponte[‡], Susan A. Charman[Δ], Karen L. White[Δ], Abhijit Kundu[◊], Surajit Sadhukhan[◊], Mel Lloyd[#], Gail M. Freiberg[∞], Myron Srikumaran[∞], Marc Siggel[†], Adrian Zwyssig[†], Pimchai Chaiyen[≡], and François Diederich[†,]*

[†]Laboratorium für Organische Chemie, ETH Zurich, Vladimir-Prelog-Weg 3, 8093 Zurich, Switzerland

[‡]BASF SE, Carl-Bosch-Strasse 38, 67056 Ludwigshafen, Germany

[§]Swiss Tropical and Public Health Institute (SwissTPH), Socinstrasse 57, 4051 Basel, Switzerland

[ø]Universität Basel, Petersplatz 1, 4003 Basel, Switzerland

[‖]Medicines for Malaria Venture, Route de Pré-Bois 20, CH-1215 Geneva, Switzerland

[⊥]National Center for Genetic Engineering and Biotechnology, 113 Thailand Science Park, Phahonyothin Road, Pathumthni 12120, Thailand

[Δ]Centre for Drug Candidate Optimisation, Monash Institute of Pharmaceutical Sciences, Monash University, 381 Royal Parade, Parkville, Victoria 3052, Australia

[◊]TCG Lifesciences Private Limited, Block BN, Plot 7, Saltlake Electronics Complex, Sector V, Kolkata 700091, West Bengal, India

[#]Covance Laboratories Ltd., Otley Road, Harrogate, HG3 1PY, United Kingdom

[∞]AbbVie, Molecular Characterization, Dept. R4AE, 1 North Waukegan Rd., N. Chicago, IL, 60064-6217

[≡]Department of Biochemistry and Center for Excellence in Protein and Enzyme Technology, Faculty of Science Mahidol University, 272 Rama VI Road, Bangkok 10400, Thailand

KEYWORDS

Malaria, Plasmodium, SHMT, drug target, structure-based design, inhibitor, pyrazolopyran.

ABSTRACT

Target-based approaches towards new antimalarial treatments are highly valuable to prevent resistance development. We report several series of pyrazolopyran-based inhibitors targeting the enzyme serine hydroxymethyltransferase (SHMT), designed to improve microsomal metabolic stability and to identify suitable candidates for *in vivo* efficacy evaluation. The best ligands inhibited *Plasmodium falciparum* (*Pf*) and *Arabidopsis thaliana* (*At*) SHMT in target assays and *Pf*NF54 strains in cell-based assays with values in the low nanomolar range (3.2–55 nM). A set of carboxylate derivatives demonstrated markedly improved *in vitro* metabolic stability ($t_{1/2} > 2$ h). A selected ligand showed significant *in vivo* efficacy with 73% of parasitemia reduction in a mouse model. Five new cocrystal structures with *Pv*SHMT were solved at 2.3–2.6 Å resolution, revealing a unique water-mediated interaction with Tyr63 at the end of the *para*-aminobenzoate channel. They also displayed the high degree of conformational flexibility of the Cys364–loop lining this channel.

INTRODUCTION

The discovery of artemisinin, the active substance of *Artemisia annua L.*, by Chinese researchers in the so-called Project 523 was a major breakthrough in the fight against Malaria in the past century.[1] This discovery was honored by the 2015 Nobel prize in Medicine awarded to Dr. Youyou Tu who led the pioneering research. Artemisinin derivatives are still the most widely used treatment, mainly in combination with other antimalarials, known as artemisinin-based combination therapy (ACT). Over the past few years, however, emergence of resistance against artemisinin and ACTs has been reported in Southeast Asia, threatening current eradication efforts.[2–4] Although mutation of the protein *P. falciparum* Kelch13 (*Pf* Kelch13) has been recently identified to be a potential key player involved in the resistance mechanism,[5–7] the fact that the mode of action and the exact target of artemisinin-based drugs are still not clearly defined makes resistance a difficult hurdle to overcome.[8] This, combined with the fact that resistance is described for most other antimalarials currently in use, renders the discovery of new targets and new treatments crucial for complete eradication of Malaria.[9]

In this respect, new inhibitors also containing a pharmacophoric peroxide bond have been developed, such as artemisone[10] and OZ439 (Figure 1), which is in phase IIa clinical trials.[11] NITD609 (Figure 1), a spiroindolone derivative, holds great promise and cleared parasitemia in adults in phase II clinical trial.[12,13] Another lead based on an imidazolopiperazine core, KAF156 (Figure 1), has just finished phase II, open-label, two-part clinical study trials after showing its potential of acting on all stages of the life cycle of the parasite, blocking transmission of parasitemia and even prophylactic activity.[14–17] Lately, novel multistage antimalarial inhibitors identified by phenotypic screening[18] and derived from diversity-oriented synthesis have shown

remarkable efficacy.[19] In addition, a selective β2 proteasome inhibitor exhibited a high curing potential with almost complete reduction of parasite burden after a single bolus dose of 35 mg kg^{-1}.[20] A target-based approach led to the discovery of DSM265 (Figure 1), an inhibitor of the enzyme dihydroorotate dehydrogenase (DHODH), which is currently in phase IIb clinical trials.[21] Finally, P218 (Figure 1), an inhibitor of the dihydrofolate reductase (DHFR) enzyme involved in the folate cycle, emerged as a viable substitute of pyrimethamine and cycloguanil, and is currently undergoing preclinical testing.[22] This portfolio of potentially new therapeutics is encouraging, however, for some of them the molecular targets remain unknown, thus prevention or identification of resistance mechanism is highly challenging.

Figure 1. Molecular structures of novel antimalarials currently investigated in clinical trials.

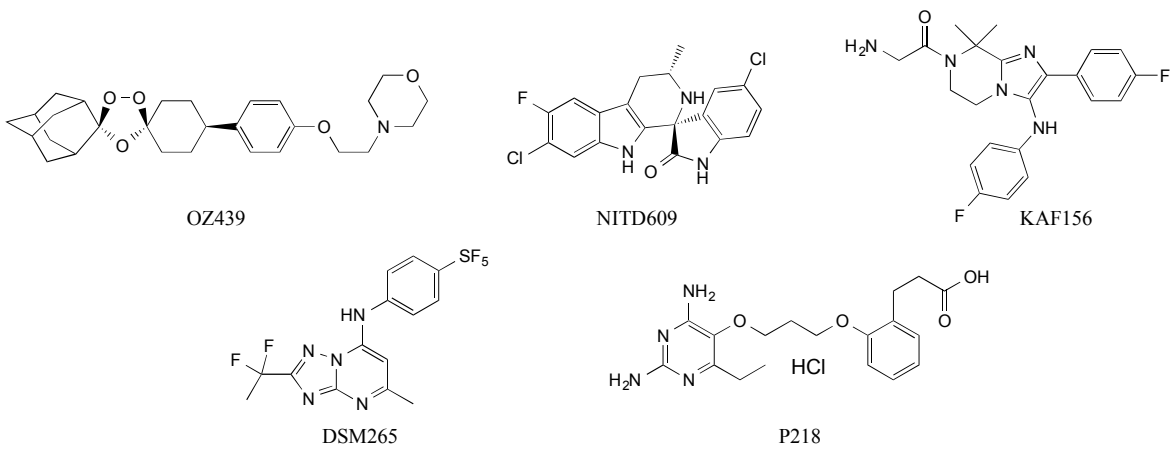

We recently demonstrated that the pyridoxal 5'-phosphate (PLP) dependent enzyme serine hydroxymethyltransferase (SHMT),[23–36] from the folate cycle,[37–39] which remarkably had been neglected so far, could be targeted by pyrazolopyran-based ligands to efficiently reduce parasitemia *in vitro* (Figure 2).[40] *Pv*SHMT has a homodimeric structure and two active sites per homodimer, where both active sites were found to be populated by a ligand (SI, Section S4.1,

Figure S11).[40] Here, we report the structure-based design and synthesis of an extended library of pyrazolopyran-based ligands, targeting improved metabolic stability. The *in vitro* metabolic stability, which was poor in the earlier reported series of ligands,[40] was improved substantially with the current ligands with *in vitro* microsomal half-lives exceeding 2 h. At the same time, on-target activity on *Plasmodium falciparum* (*Pf*) SHMT and *Arabidopsis thaliana* (*At*) SHMT (used to refine the SAR) as well as *in vitro* activity against the *Pf*NF54 sensitive strain were maintained in the low nanomolar IC_{50} (half maximal inhibitory constant) and EC_{50} (half maximal effective concentration) ranges, respectively. No apparent cytotoxicity of the improved leads was observed. We show for the first time that SHMT inhibitors can be effective *in vivo*. One of the most promising candidates has been advanced to an *in vivo* mouse model. Gratifyingly, a significant reduction of parasitemia of 73% was measured compared to untreated mice at 4 × 50 mg/kg (p.o.). Additionally, five new cocrystal structures were solved, confirming the binding mode of the pyrazolopyran-based ligands. A detailed investigation of the molecular recognition properties at the active site of *Pv*SHMT was undertaken, revealing an interesting water-mediated interaction with Tyr63 at the end of the channel, where the *para*-aminobenzoate side chain of the substrate tetrahydrofolate (THF) binds. The particular conformational flexibility of the Cys364–loop lining this channel was analyzed as well. It should be noted that there has also been recent interest in human SHMT as a potential new cancer target.[41–43]

Figure 2. a) The folate cycle.[a] b) Molecular structure of tetrahydrofolate (THF). c) Schematic depiction of the binding mode of the initial lead (+)-**1** as seen in a cocrystal structure analysis (PDB ID: 4TMR).[40] Intermolecular H-bonding are indicated by red dashed lines.

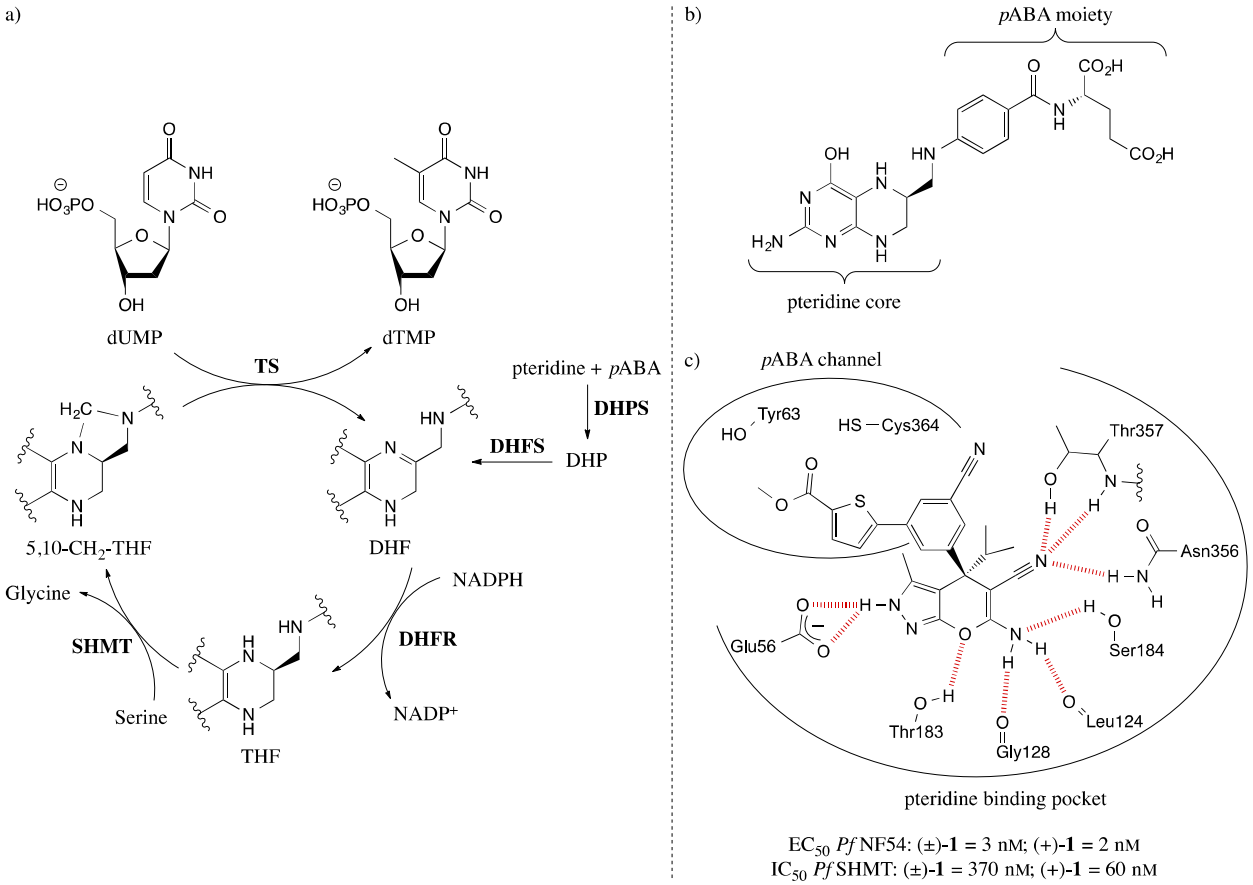

[a]Serine hydroxymethyltransferase (SHMT) converts tetrahydrofolate (THF) to 5,10-methylenetetrahydrofolate (5,10-CH_2-THF), a crucial component for the conversion of deoxyuridine monophosphate (dUMP) to the DNA precursor deoxythymidine monophosphate (dTMP) by thymidylate synthase (TS). Dihydrofolate (DHF) formed by this process is converted back to THF by dihydrofolate reductase (DHFR). In *Plasmodium*, components of the cycle are replenished by *de novo* synthesis: dihydropteroate synthase (DHPS) condenses pteridine diphosphate and *para*-aminobenzoic acid (*p*ABA) to dihydropteroate (DHP), which is converted to DHF by dihydrofolate synthase (DHFS).

RESULTS AND DISCUSSION

Ligand Design

The first generation ligands, such as (+)-**1**, showed high activity in cell-based assays against *Pf*NF54 and various drug-resistant mutant strains, as well as very low cytotoxicity. Their metabolic stability however was insufficient, and exposure was unlikely to be sufficient to achieve *in vivo* efficacy.[40] Improving metabolic stability was therefore necessary to advance this program, and structural changes of the ligands was guided by structure-based design based on the two cocrystal structures that had been obtained. Figure 2c schematically shows the binding mode of (+)-**1** at the active site of *Pv*SHMT (PDB ID: 4TMR). Two sub-pockets are distinguishable. The pteridine pocket, which binds the pyrazolopyran core and also the pteridine core of THF by several H-bonds to the protein (PDB ID: 4OYT), whereas an extended channel hosts the biaryl motif of (+)-**1** and the *p*ABA side chain of THF. In the new ligand series, the pyrazolopyran core was kept intact, whereas its alkyl substituents and in particular the biaryl moiety attached to the stereogenic center were systematically altered based on computational predictions using the modeling software MOLOC.[44] These ligand alterations are reported in the following.

Synthesis and Cell-based Activity of Thiophene Derivatives (±)-2–27

Methyl ester (±)-**1**, identified in a primary screening of ligands and initially developed as potential herbicide targeting *At*SHMT,[45] was found to have a poor metabolic stability when incubated with human liver microsomes ($t_{1/2}$ = 3 min). As there was evidence of ester cleavage in (±)-**1**, we first focused on the replacement of this moiety aiming at maintaining EC_{50}-values against *Pf*NF54 strain in the single digit nanomolar range.[40] The ligands (±)-**2**–**8** (Scheme 1)

were synthesized in 5–6 steps starting from **9**/**10**. The key steps are a Suzuki-Miyaura cross-coupling[46] to **11a**–**g**, a Knoevenagel condensation to **12a**–**g**, and a Michael addition of 3-methyl-2-pyrazolin-1-one, followed by an intramolecular cyclization to provide (±)-**2**–**8** (for more details, see the Supporting Information Section S1).

Scheme 1. Representative Synthesis of Pyrazolopyran Ligands (±)-**2**–**8**.[a]

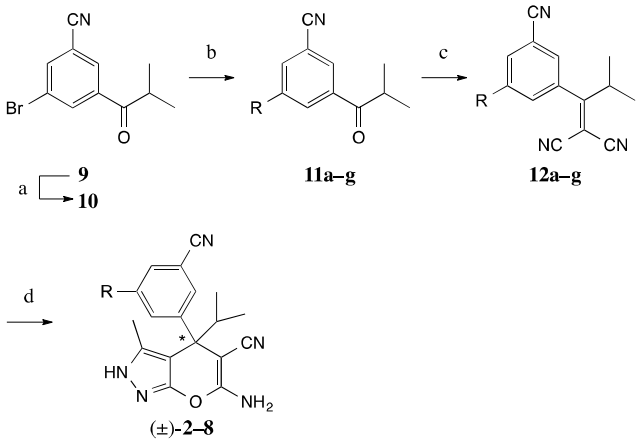

[a]Reagents and conditions: (a) bis(pinacolato)diboron, KOAc, $[PdCl_2(dppf)\cdot CH_2Cl_2]$ (2.0 mol %), toluene, μw, 150 °C, 6 min; (b) thienyl boronic acid or bromothiophene analogue, $[PdCl_2(PPh_3)_2]$ (5.0 mol %), Na_2CO_3, THF/H_2O 4:1, 60 °C, 4–16 h; (c) malononitrile, $TiCl_4$, pyridine, $CHCl_3$, 63 °C, 48–72 h; (d) 3-methyl-2-pyrazolin-1-one, piperidine, 1,4-dioxane/EtOH 1:1, μw, 65 °C, 3.5 h.

Ligands (±)-**2**, **3**, and **5** displayed moderate affinities for *Pf*SHMT, whereas oxadiazole (±)-**6** and sulfonamide (±)-**7** analogues gave better inhibition with IC_{50} values in the low three digit nanomolar range (Table 1). Higher affinity was achieved with the methoxymethyl ether (±)-**4** (IC_{50} = 42 nM). Based on these results, the benzothiophene analogue (±)-**8** was designed with the intention of maintaining the S···S interaction[47,48] to Cys364 and improving the hydrophobic interactions with the surrounding residues as Tyr63 and Phe266 (SI, Section S3, Figure S9a). The predicted interactions nicely led to an improved IC_{50} value of 60 nM. Cocrystal structures of

(±)-**4** and (±)-**7** with *Pv*SHMT, which features a virtually identical active site to *Pf*SHMT,[35] were obtained. The overall binding mode seen for complexed (+)-**1** was confirmed. However, no good explanation became apparent for the higher target affinity of (±)-**4** as compared, for example, to (±)-**3** (SI, Section S4.3, Figure S15 and S16). The methoxymethyl ether moiety is located at the exit of the *p*ABA channel at the periphery of the protein, it is turned out of the plan compared to the ester group in (+)-**1** (C–C–C–O torsion angle = 69°) and does not directly interact with any protein residue. Regarding (±)-**7**, its sulfonamide moiety is found in the preferred staggered conformation, with the *N*-lone pair bisecting the O=S=O fragment[49] and at a 3.7 Å distance of Tyr63, is too far away to establish a strong polar interaction (SI, Section S4.3, Figure S17). On the other hand, one of the *N*-methyl groups is at 3.1 Å to the edge of Phe134 leading to a short C–H···π contact and two short O···H–C contacts are established between one S=O bond and Val141 and Pro267 (SI, Section S4.3, Figure S18).

Table 1. Biological Activities of Thiophene Derivatives (±)-2–8.

Num.	R	EC_{50} *Pf* NF54 [nM]	IC_{50} *Pf* SHMT ± SD [nM][a]
(±)-**2**	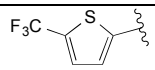	594	388 ± 5
(±)-**3**	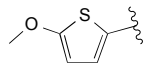	410	323 ± 43
(±)-**4**	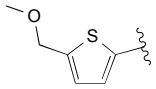	228	42 ± 1
(±)-**5**	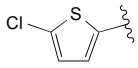	501	202 ± 9
(±)-**6**	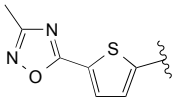	212	133 ± 6
(±)-**7**	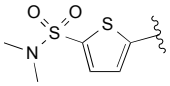	151	99 ± 2
(±)-**8**	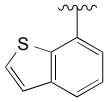	197	60 ± 1

[a]Standard deviations are given.

Overall there was a good correlation between the target-based and the *Pf*NF54 cell-based assay. In this assay, the best inhibitor of the series was sulfonamide (±)-**7** with an EC_{50} value of 151 nM (Table 1).

Since the cell-based affinity of this series of thiophene derivatives was still two orders of magnitude lower than that of (±)-**1** (EC_{50} value = 3 nM), modifications at other positions of the molecule were evaluated to improve biological activity. Table 2 gives the EC_{50} values for the cell-based assay which vary by more than a factor of 600. The IC_{50} values in the *Pf*SHMT target assay, however, were all very similar, in the triple-digit nanomolar range, possibly due to a limited dynamic range of the assay in particular at higher binding affinity. All IC_{50} values for *Pf*SHMT are given in Table S1 in the SI, together with the IC_{50} values of selected compounds measured against *At*SHMT, which correlate much better with the EC_{50} data. *Arabidopsis thaliana* SHMT, the plant counterpart and *Pf*SHMT are highly similar with 45% of sequence identity, and only very few amino acid residues differ within each active site (SI, Section S4.2, Figures S12, S13 and S14).[45] Many of the SARs established in the following from the cell-based assay data are nicely supported by the *At*SHMT target assay data.

For comparison, ligand (±)-**5** (Table 1) was chosen as reference compound. We first investigated changes of the *meta* substituent on the biaryl phenyl ring. Substitution of the nitrile in (±)-**5** by a chloride ((±)-**13**) or bromide ((±)-**14**) did not have significant effect (Table 2). Introduction of a CF_3 group ((±)-**15**) resulted in an improved *in vitro* potency by a factor of 2 (EC_{50} = 226 nM).

Table 2. Structure-Activity Relationships for Positions R^2, R^3, and R^4.

Num.	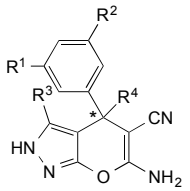				EC_{50} *Pf* NF54 [nM]
	R^1	R^2	R^3	R^4	
(±)-**13**	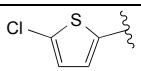	Cl	Me		485
(±)-**14**	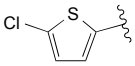	Br	Me		892
(±)-**15**	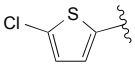	CF_3	Me		226
(±)-**16**	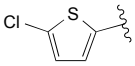	OCF_3	Me		3760
(±)-**17**	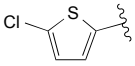		Me		7106
(±)-**18**	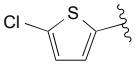		Me		4511
(±)-**19**	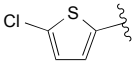		Me		5501
(±)-**20**	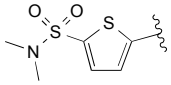	CF_3	Me		18
(±)-**21**	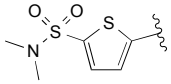	CF_3	CD_3		11
(±)-**22**	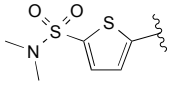	CF_3	Et		172
(±)-**23**	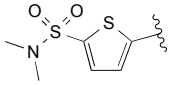	CF_3	*cy*Pr		576
(±)-**24**	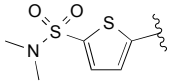	CF_3	H		29
(±)-**25**	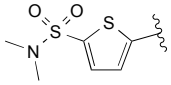	CF_3	Me		340
(±)-**26**	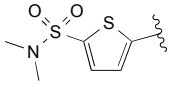	CF_3	Me		1202
(±)-**27**	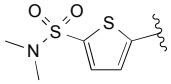	CF_3	Me		498

With larger substituents, the potency was significantly reduced and EC_{50} values in the single-digit micromolar range were measured ((±)-**16**–**19**). The larger groups interfere with the

conformationally flexible Cys364–loop, which was only discovered later and is discussed below based on new cocrystal structures.

Gratifyingly, by applying the CF_3-substitution to the sulfonamide ligand (±)-**7**, a low nM cell-based activity could be reached, giving more than a 10-fold boost in potency (EC_{50} (±)-**20** = 18 nM). Encouraged by this result, we investigated positions R^3 and R^4 on the pyrazolopyran core in the sulfonamide ligand series, preparing ligands (±)-**21**–**27**. In position 3, the methyl substituent was optimal, and its potency only rivaled by a CD_3- (EC_{50} (±)-**21** = 11 nM) or a H-substituent (EC_{50} (±)-**24** = 29 nM). Ethyl and cyclopropyl substituents in this position were detrimental to activity.

Study of the substituent R^4 at the stereogenic center revealed that this position was not amenable to broad changes. Substitution of the isopropyl in (±)-**20** (EC_{50} = 18 nM) by ethyl, cyclopropyl, and cyclobutyl ((±)-**25**–**27**) strongly reduced the cell-based activity (Table 2). The preference for R^3 = Me and R^4 = $CH(CH_3)_2$ undoubtedly are target-binding related as could be validated by the set of 7 cocrystal structures obtained so far in the project. Although (±)-**20** had promising antiparasitic activity, it was not further pursued due to its poor liver microsomal stability ($t_{1/2}$ = 3 min; SI, Section S2.2, Table S2). Instead, identification of potential metabolites was performed in order to guide the next round of optimization.

Identification of Metabolites from (±)-20

Metabolite identification performed on (±)-**20** in NADPH-supplemented human liver microsomes revealed major degradation pathways *via* thiophene oxidation and *N*-demethylation accounting for approximately 50 and 33% of total metabolites, respectively (SI, Section S2.4, Tables S5 and S6). The results were confirmed by an isotopic labeling experiment using the

deuterated analogue (±)-**21**, enabling exclusion of potential metabolism on the methyl-pyrazole moiety (SI, Section S2.4, Tables S7 and S8). A previously reported ligand (±)-**28**,[40] lacking the thiophene moiety and featuring a 3,5-dichlorophenyl substituent at the stereogenic center (for the structure, see SI, Figure S5), was studied as well. For this compound, the main metabolite arises from oxidation on the pyrazolopyran core, possibly by oxidation of the vinylogous cyanamide (SI, Section S2.4, Figure S5 and Tables S9 and S10). These results suggested that metabolism is compound-specific and that the vinylogous cyanamide moiety might be a liability. However, we focused during the further optimization on the replacement of the substituted-thiophene peripheral part to prepare more stable ligands.

Heteroalicyclic Rings as Thiophene Replacements

In an effort to identify suitable thiophene replacements with the goal to achieve high *in vitro* potency, a series of 13 inhibitors featuring *N*-heteroalicycles of various sizes and different nature were synthesized. The terminal rings in (±)-**29**–**37** were selected to both maintain hydrophobic interactions with the surrounding residues in the *p*ABA channel and reduce the overall lipophilicity of the molecule. Ligands (±)-**29**–**37** were prepared by employing a Buchwald-Hartwig cross-coupling[50] between the building block **38** and the corresponding secondary amines to give **39a**–**i**, followed by the classical two-steps sequence *via* **40a**–**i** leading to the final pyrazolopyran analogues (Scheme 2).

Scheme 2. Synthesis of Ligands (±)-29–37 Employing a Buchwald-Hartwig Cross-Coupling.[a]

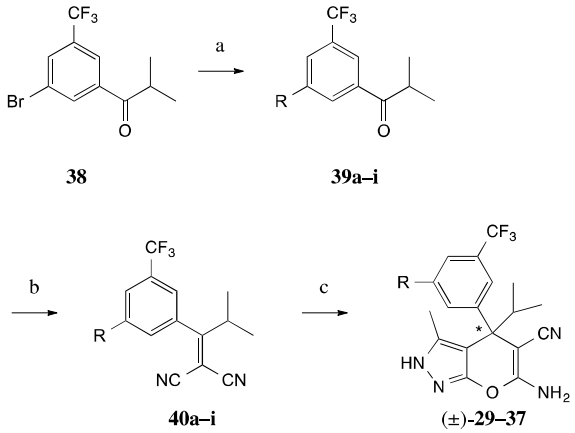

[a]Reagents and conditions: (a) corresponding secondary amine, Cs_2CO_3, $[Pd_2(dba)_3]$ (2.0 mol %), X-Phos (8.0 mol %), 1,4-dioxane, 110 °C, 16 h; (b) malononitrile, $TiCl_4$, pyridine, $CHCl_3$, 63 °C, 48–72 h; (c) 3-methyl-2-pyrazolin-1-one, piperidine, 1,4-dioxane/EtOH 1:1, μw, 65 °C, 3.5 h.

As the *N*-heterocyclic derivatives (±)-**29**–**37** lack functional groups able to interact with Cys364, sultam (±)-**41** was designed to establish chalcogen interactions (S···O)[47] with this residue. The synthesis started with the conversion of **38** to Boc-protected **42** and aniline **43**. Subsequent treatment with 4-chloro-butane-1-sulfonyl chloride afforded the sultam precursor **44**, which underwent Knoevenagel condensation to **45** and core formation, yielding (±)-**41** (Scheme 3).

Scheme 3. Synthesis of Sultam (±)-41.[a]

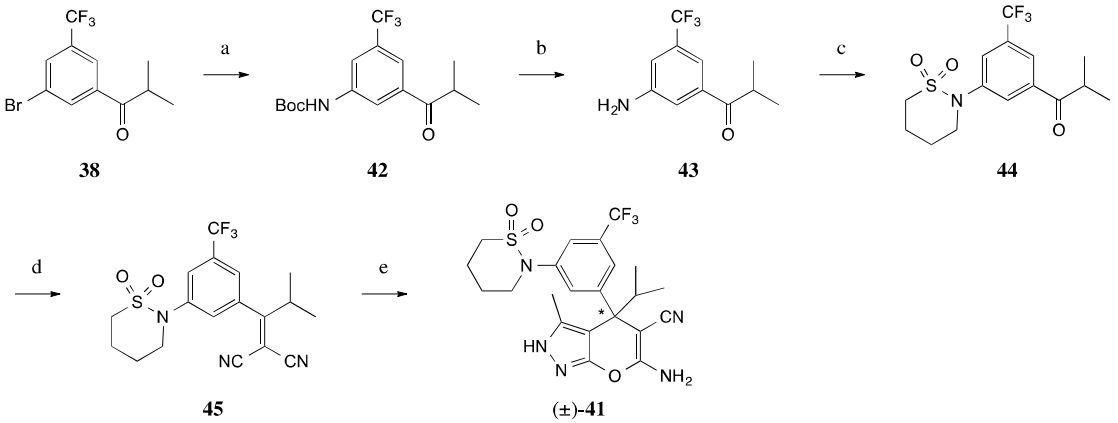

[a]Reagents and conditions: (a) *tert*-butyl carbamate, Cs_2CO_3, $[Pd_2(dba)_3]$ (2.0 mol %), X-Phos (8.0 mol %), 1,4-dioxane, 110 °C, 16 h, 40%; (b) TFA, CH_2Cl_2, 25 °C, 3 h, 71%; (c) 4-chloro-butane-1-sulfonyl chloride, Et_3N, CH_2Cl_2, 25 °C, 4 days, 47%; (d) malononitrile, $TiCl_4$, pyridine, $CHCl_3$, 63 °C, 48 h, 66%; (e) 3-methyl-2-pyrazolin-1-one, piperidine, 1,4-dioxane/EtOH 1:1, μw, 65 °C, 3.5 h, 39%.

Another sulfone-containing inhibitor (±)-**46** with a thiadiazinane scaffold as a more polar derivative of (±)-**41** was also synthesized. The sulfamoyl carbamate was introduced by reacting **43** with the isocyanate **47** to give **48**, which was transformed into **49** by a di-*N*-alkylation of **48** with 1,3-dibromopropane/K_2CO_3 (Scheme 4). Boc-cleavage followed by *N*-methylation gave **50**, which was transformed *via* **51** into (±)-**46**. *N*-methylpyrimidone analogue (±)-**52** was also prepared with the intention to establish a contact with Cys364, as well as increasing the solubility of the inhibitor. It was synthesized following the synthetic route shown in Scheme 1.

Scheme 4. Synthesis of Thiadiazinane (±)-46.[a]

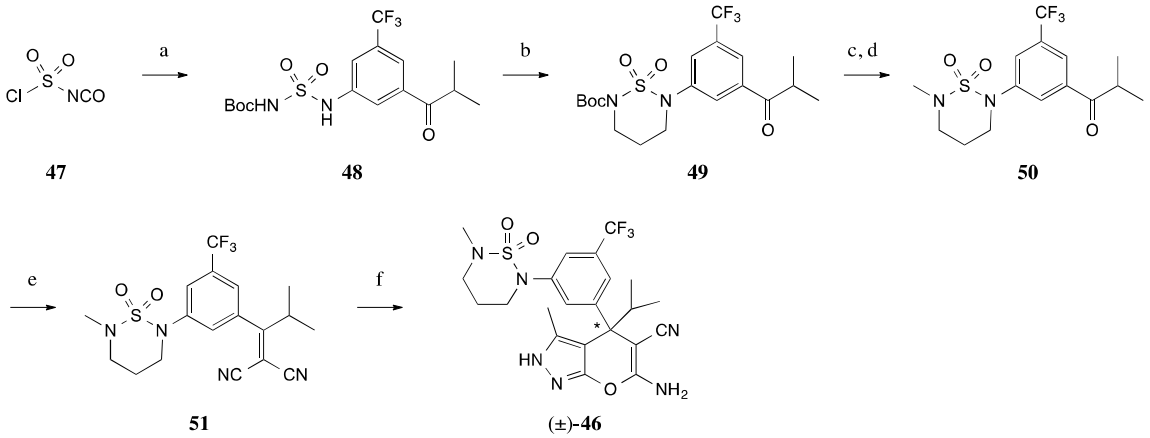

[a]Reagents and conditions: (a) *tert*-BuOH, CH_2Cl_2, 0 °C, 30 min, then **43**, Et_3N, CH_2Cl_2, 25 °C, 16 h, 80%; (b) 1,3-dibromopropane, K_2CO_3, CH_3CN, reflux, 16 h, 55%; (c) TFA, CH_2Cl_2, 25 °C, 3 h, 79%; (d) MeI, K_2CO_3, DMF, 25 °C, 3 h, 92%; (e) malononitrile, $TiCl_4$, pyridine, $CHCl_3$, 63 °C, 48 h, 55%; (f) 3-methyl-2-pyrazolin-1-one, piperidine, 1,4-dioxane/EtOH 1:1, μw, 65 °C, 3.5 h, 29%.

Ligand (±)-**53** was designed to interact with Tyr63 *via* its sulfonamide moiety. Its synthesis started from the commercially available Boc-protected iodoazetidine **54**, which was transformed into organo-zinc derivative **55** *in situ*, prior to a Negishi cross-coupling reaction[51] reaction with **38** (Scheme 5) to give **56**. The desired ligand (±)-**53** was subsequently obtained *via* sulfonamides **57** and **58**.

Scheme 5. Synthesis of the (Methanesulfonyl)azetidine (±)-53.[a]

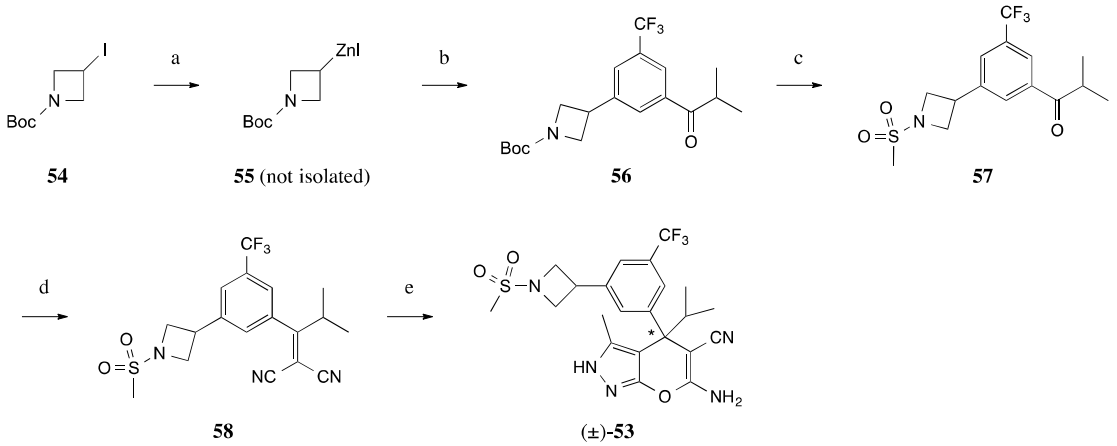

[a]Reagents and conditions: (a) Zn, 1,2-dibromoethane, DMA, 70 °C, 30 min, then chlorotrimethylsilane, DMA, 25 °C, 2 h, and 50 °C, 2 h; (b) **38**, $[Pd_2(dba)_3]$ (2.0 mol %), tri(2-furyl)phosphine (4.0 mol %), DMA, 70 °C, 20 h, 56%; (c) conc. HCl, MeOH, 25 °C, 3 h, then methanesulfonyl chloride, CH_2Cl_2, 25 °C, 12 h, 35% (over 2 steps); (d) malononitrile, $TiCl_4$, pyridine, $CHCl_3$, 63 °C, 48 h, 59%; (e) 3-methyl-2-pyrazolin-1-one, piperidine, 1,4-dioxane/EtOH 1:1, μw, 65 °C, 3.5 h, 30%.

The inhibitors of this series had EC_{50} values in the cellular assay in the 25–610 nanomolar range (Table 3). The measured IC_{50} values against *Pf*SHMT varied between 84–398 nM, and again the IC_{50} values obtained for selected inhibitors against *At*SHMT correlated much better with the data from the cell-based assay (SI, Section S2.1, Table S1). The highest cellular potency was measured for the fused *N*-heterocyclic derivatives (±)-**30**–**35**, suggesting the establishment of good hydrophobic interactions with the apolar surface at the exit of the *p*ABA channel, formed by Leu124, Leu130, Phe134, and Val141 within the active site as illustrated for the difluoroazetidine derivative (±)-**30** in Figure S9b (see SI, Section S3). In the *At*SHMT assay, compound (±)-**33** was the most potent with an IC_{50} value of 17.7 nM.

Attempts to gain affinity by interacting with Cys364 apparently remained unsuccessful ((±)-**41**, (±)-**46**, and (±)-**52**) according to both EC_{50} and IC_{50} values (SI, Section S2.1, Table S1). Sulfone

(±)-**37** and sulfonamide (±)-**53** gave both promising EC_{50} (65 nM) and IC_{50} values (*Pf*SHMT: 127 and 84 nM; *At*SHMT: 43 and 31 nM) and we took this as a lead for establishing H-bonding interactions with Tyr63, which had been suggested by the modeling (see the carboxylic acid ligand series below).

Table 3. Biological Activities of Inhibitors (±)-29–37, (±)-41, (±)-46, and (±)-52,53.

Num.	R	EC_{50} *Pf* NF54 [nM]
(±)-**29**		350
(±)-**30**	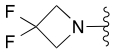	44
(±)-**31**		56
(±)-**32**	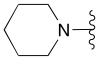	59
(±)-**33**	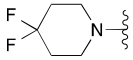	25
(±)-**34**	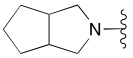	49
(±)-**35**	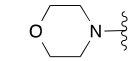	26
(±)-**36**	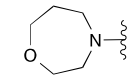	193
(±)-**37**	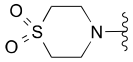	65
(±)-**41**	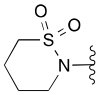	454
(±)-**46**	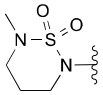	523
(±)-**52**	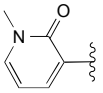	610
(±)-**53**	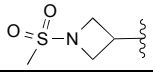	65

Aromatic *N*-Heterocyclic Ligands

In parallel to the previous series of inhibitors, and in a permanent effort towards reaching single-digit nanomolar activity, we investigated a larger set of aromatic *N*-heterocyclic derivatives ((±)-**59**–**71**). The scaffolds were synthesized by a Suzuki-Miyaura cross-coupling[46] between building block **38** (or its borylated analogue) and the respective aromatic *N*-heterocycles as shown in Scheme 1. The cell-based activities for selected ligands are summarized in Table 4. The complete biological characterization for all aromatic *N*-heterocyclic ligands is provided in the Supporting Information (Section S2.1, Table S1). The *in vitro* activities of many of the prepared compounds gave values in the low nanomolar range. Gratifyingly, five of the prepared pyridine derivatives gave the desired EC_{50} values in the single-digit nanomolar range ((±)-**60**,**61** and (±)-**67**–**69**) (Table 4) and similar activity was also measured in the *At*SHMT assay (SI, Section S2.1, Table S1).

Table 4. Biological Activities of Selected *N*-Heterocyclic Ligands (±)-59–71.

Num.	R	EC_{50} *Pf* NF54 [nM]
(±)-**59**	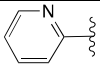	115
(±)-**60**	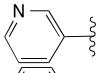	4.8
(±)-**61**	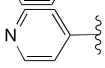	3.2
(±)-**62**	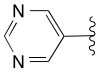	10
(±)-**63**	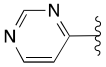	27
(±)-**64**	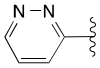	125
(±)-**65**	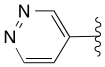	18
(±)-**66**	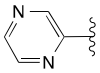	52
(±)-**67**	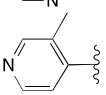	4.2

(±)-**68**	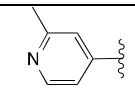	5.1
(±)-**69**	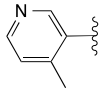	6.4
(±)-**70**	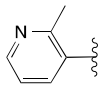	14
(±)-**71**	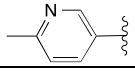	66

No apparent cytotoxicity for (±)-**60** and (±)-**61** was measured on rat myoblast cell line (L6) and human HepG2 cell line, with IC_{50} values only in the high micromolar range (SI, Sections S2.7 and S2.8, Tables S23 and S24). hERG inhibition was also assessed for (±)-**60**, resulting in an IC_{50} of 29 μM which highlights once again the safeness of this series (SI, Section S2.8, Table S24). The potential of these ligands however was greatly diminished by their very short half-life when incubated with human liver microsomes (< 10 min) (SI, Section S2.2, Table S2). Despite this liability, the high antiparasitic efficacy of (±)-**61** prompted us to further study its antiplasmodial activity in a *P. falciparum* SCID (severe combined immunodeficiency) mouse model[52] at 4 × 50 mg/kg (p.o.). The rather low 25% parasitemia reduction is possibly the result of poor exposure due to high metabolic instability of (±)-**61** (SI, Section S2.9, Figure S7, Tables S25 and S26).

Carboxylic Acid Series

While measuring the metabolic stability of selected ligands previously reported,[40] carboxylic acid derivative (±)-**72** drew our attention as it was reasonably stable in the microsomal test system ($t_{1/2}$ = 137 min), but had only moderate potency (EC_{50} *Pf* NF54 = 340 nM) (Table 5). Subsequently, we put our effort onto improving the antiparasitic efficacy of this carboxylic acid analogue, while maintaining a high microsomal stability, using the knowledge learned from the

previous optimization cycles by replacing the *meta*-CN on the phenyl ring at the stereogenic center with a *meta*-CF_3 group or inserting an *N*-heterocycle for instance.

Table 5. Biological Activities, log$D_{7.4}$ Values, and Microsomal Half-Lives of Carboxylate-Based Ligands (±)-72–79.

Num.	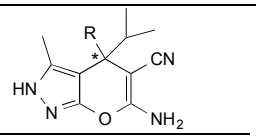 R	EC_{50} *Pf* NF54 [nM]	IC_{50} *Pf* SHMT ± SD [nM][a]	IC_{50} *At* SHMT [nM]	log$D_{7.4}$[b]	$t_{1/2}$ [min][c]
(±)-**72**	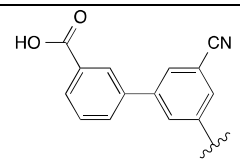	340	220 ± 70	0.088	1.4	137
(±)-**73**	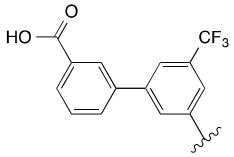	54	189 ± 7	19.1	1.8	41
(±)-**74**	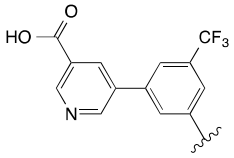	632	119 ± 6	n.d.[d]	n.d.	64
(±)-**75**	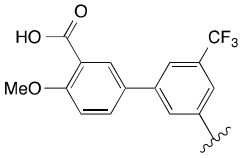	822	77 ± 1	n.d.	1.7	59
(±)-**76**	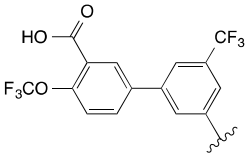	172	268 ± 15	n.d.	n.d.	70
(±)-**77**	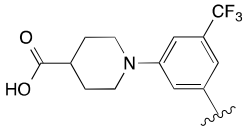	116	312 ± 10	41.9	1.6	55
(±)-**78**	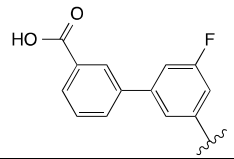	194	56 ± 1	27.8	1.5	157

(±)-**79**	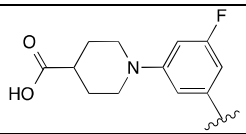	154	75 ± 1	26.2	1.2	226

[a]Standard deviations are given. [b]Measured by HPLC, for the method see the SI, Section S2.2. [c]*In vitro* metabolic stability measured in human liver microsomes. [d]n.d. = not determined.

We prepared a series of *meta*-CF_3 derivatives (±)-**73**–**77** (Table 5) and as expected, substitution of the cyano moiety in (±)-**72** by a CF_3 group (EC_{50} (±)-**73** = 54 nM) helped to improve cell-based potency, though at the expense of its metabolic stability (Table 5). All other prepared derivatives, with either a terminal aromatic ring or an *N*-linked piperidine, gave mixed results, when considering all parameters including target affinity, cell-based affinity and microsomal half-life. Also the piperidine derivatives showed good solubility (for solubility measurements of selected ligands, see the SI, Section S2.3, Table S3). Examining the log$D_{7.4}$ value of (±)-**72** and (±)-**73** (1.4 and 1.8, respectively, Table 5), we reasoned that a compound having lipophilicity in this range would be likely to lead to a good balance between potency and stability. Indeed, the *meta*-fluoro derivative (±)-**78** has a moderate activity on *Pf*NF54 (EC_{50} = 194 nM), but to our delight, it surpassed all ligands studied so far with a microsomal half-life of 157 min. Ligand (±)-**78** was also incubated in rat liver microsomes resulting in a comparable half-life of 95 min (SI, Section S2.2, Table S2). This step forward in the pursuit of metabolically stable inhibitor was further confirmed in an *in vivo* rat model, in which an apparent *in vivo* half-life of 3 h was measured (SI, Section S2.5). The difference between *in vitro* and *in vivo* half-lives can possibly be attributed to plasma protein or microsome binding. Noticeably, applying the CF_3→F replacement strategy to piperidine derivative (±)-**77** led to a slight potency loss, which was compensated by a large stability gain ((±)-**79**). In addition (±)-**78** and (±)-**79** had high target affinity in both *Pf*SHMT and *At*SHMT assays.

We subsequently prepared ligands (±)-**80**–**87** with carboxylate side chains of larger length (Table 6). The cocrystal structure of the natural substrate THF bound to SHMT (PDB ID: 4OYT, 2.4 Å) shows the two carboxylates of its terminal glutamate located at the exit of the *p*ABA channel at the periphery of the binding pocket. Overlaying this previously reported cocrystal structure of THF with *Pv*SHMT[36] and the modeled carboxylic acid derivative (+)-**85** clearly suggested that extension of the carboxylate chain might allow to better mimic the THF side chain, thus eventually improving the potency (SI, Section S3, Figure S10).

Table 6 indeed shows that extension of the carboxylate side chain has a beneficial effect on cellular potency in both CF_3- and F-series (*e.g.*: EC_{50} values (±)-**77** (116 nM) > (±)-**82** (84 nM) > (±)-**83** (17 nM); or (±)-**79** (154 nM) > (±)-**86** (55 nM) > (±)-**87** (17 nM)). Activity gain came along with a loss in metabolic stability, which became unacceptable in the CF_3 series.

Table 6. Biological Activities and Microsomal Half-Lives of Ligands (±)-80–87 with Extended Carboxylate Side Chains.

Num.	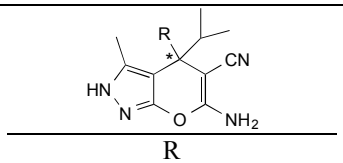 R	EC_{50} *Pf*NF54 [nM]	IC_{50} *Pf*SHMT ± SD [nM][a]	IC_{50} *At*SHMT [nM]	$t_{1/2}$ [min][b]
(±)-**80**	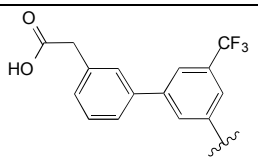	22	186 ± 9	59.0	54
(±)-**81**	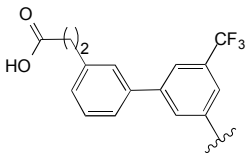	10	165 ± 7	27.0	31
(±)-**82**	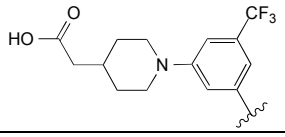	84	186 ± 7	13.5	36

(±)-**83**	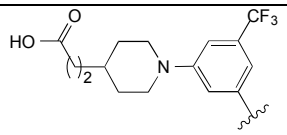	17	168 ± 11	18.2	12
(±)-**84**	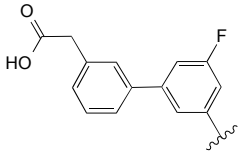	52	172 ± 10	22.4	159
(±)-**85**	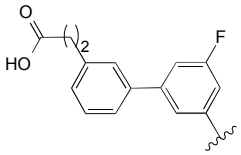	19	90 ± 4	33.6	95
(±)-**86**	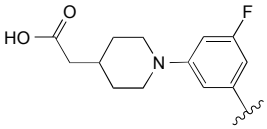	55	97 ± 1	37.1	194
(±)-**87**	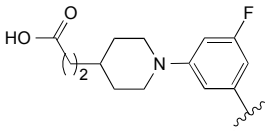	17	130 ± 4	13.8	50

[a]Standard deviations are given. [b]*In vitro* metabolic stability measured in human liver microsomes.

As acidic ligands tend to have a high plasma protein binding,[53] this parameter was measured *via* ultracentrifugation in mouse plasma for the highly potent ligand (±)-**81** and the most stable analogue (±)-**86**. Significant differences were observed as (±)-**81** was highly bound to plasma proteins (99.2% bound), whereas (±)-**86** had much lower binding (82.9% bound) (SI, Section S2.10, Table S29). Taking all parameters into account, (±)-**86** was clearly the compound with the most attractive profile and the best balance between potency and metabolic stability.

Encouraged by these results we investigated the pure enantiomers of (±)-**86**. For this purpose, the enantiomers of the direct precursor to (±)-**86** were separated by chiral HPLC and subsequent hydrogenation afforded pure (+)-**86** and (–)-**86** (see Scheme 6 in the Experimental Section and HPLC traces in the SI, Section 1.10). As observed previously with enantiomerically pure pyrazolopyran-based ligands,[40] (+)-**86** is considerably more potent than (–)-**86** in all *in vitro* assays (Table 7). This large discrepancy can be easily rationalized by the preferred binding mode

of pyrazolopyran-based ligands; as for all analogues cocrystallized with *Pv*SHMT, exclusively the (+)-enantiomers where found to be bound to the enzyme as detailed below. Additionally, (+)-**86** is roughly two-fold more potent than the racemic mixture. Remarkably, (+)-**86** also has an improved metabolic stability with a *in vitro* half-life greater than 255 min.

Table 7. Biological Activities and Microsomal Half-Lives of Enantiopure Ligands (+)-86 and (–)-86.

Num.	EC_{50} *Pf*NF54 [nM]	IC_{50} *Pf*SHMT ± SD [nM][a]	IC_{50} *At*SHMT [nM]	$t_{1/2}$ [min][b]
(±)-**86**	55	97 ± 1	37.1	194
(+)-**86**	35	110 ± 2	12.6	>255[c]
(–)-**86**	6143	1581 ± 49	977	206

[a]Standard deviations are given. [b]*In vitro* metabolic stability measured in human liver microsomes. [c]This compound showed minimal degradation (<15%) over the course of the incubation.

Cytotoxicity and Mutagenicity Evaluation

Cytotoxicity of selected compounds from each series studied above was determined against rat myoblast L6-cells in a 72 h cytotoxicity assay (SI, Section S2.7, Table S23). All ligands showed excellent selectivity indexes, with IC_{50} values ranging from 9.9 to >200 μM. Also, (±)-**60** was tested in the human HepG2 cell line resulting in an IC_{20} of 18.9 μM (SI, Section S2.8, Table S24).

Mutagenicity was addressed *via* an AMES assay[54] employing (±)-**78** as reference compound, with and without metabolic activation. Out of the 5 strains examined, reproducible evidence of mutagenicity (≥2-fold increase in revertant colony numbers over concurrent vehicle controls) was observed only in strain TA98 without metabolic activation at 5000 μg/plate in Experiment 1

and at 1250 μg/plate and above in Experiment 2, using the plate incorporation method (SI, Section S2.6).

Animal Model

The promising properties of ligand (+)-**86** prompted us to study its *in vivo* efficacy in a *P. falciparum* SCID mouse model[52] at 4 × 50 mg/kg (p.o.). Administration of (+)-**86** on days 3, 4, 5, and 6 after infection led to a significant reduction of parasitemia of 73% (vs. untreated mice) on day 7 after infection (SI, Section S2.9, Figure S8, Tables S27 and S28). Albeit complete clearance was not reached, this positive result provides a true proof of concept and validates SHMT a viable *in vivo* antimalarial target. Encouraged by this outcome, we plan to further develop this series of inhibitors in order to completely reduce parasitemia *in vivo*. Complete determination of the pharmacokinetic profile and measurement of the *in vivo* exposure will give valuable insight for improving efficacy.

Crystal Structure Determination of *Pv*SHMT with (±)-4, (±)-7, (±)-80, (±)-81, and (±)-85.

*Pv*SHMT was crystallized from the ternary complex of *Pv*SHMT, glycine, and either (±)-**4**, (±)-**7**, (±)-**80**, (±)-**81**, or (±)-**85** using the microbatch method. The cocrystals diffracted to 2.6, 2.3, 2.3, 2.3, and 2.3 Å resolution, respectively, and belong to the *C*2 space group. The structures were solved by molecular replacement using the coordinates of a chain A protomer of *Pv*SHMT (PDB code 4OYT) as the template.[36] Despite using a racemic mixture of ligands for cocrystallization, only the (+)-enantiomer was present in the structure.

Figure 3. Cocrystal structure (PDB ID: 5GVN, 2.3 Å resolution) showing the protein-ligand interactions of pyrazolopyran (+)-**85** (lime) and *Pv*SHMT (grey). a) Occupancy of the active site by (+)-**85**, the water-mediated interaction with Tyr63, and the cofactor (pyridoxal 5'-phosphate, PLP). The mesh spans the volume of the binding pocket. b) Polar interactions between (+)-**85** and the protein; PLP is omitted for clarity. The water molecules (W1, W2, and W3) are represented as red spheres. Distances are given in Å. Color code: $C_{protein}$ grey, C_{Ligand} lime, C_{PLP} yellow, F light cyan, N blue, O red, P orange, S yellow.

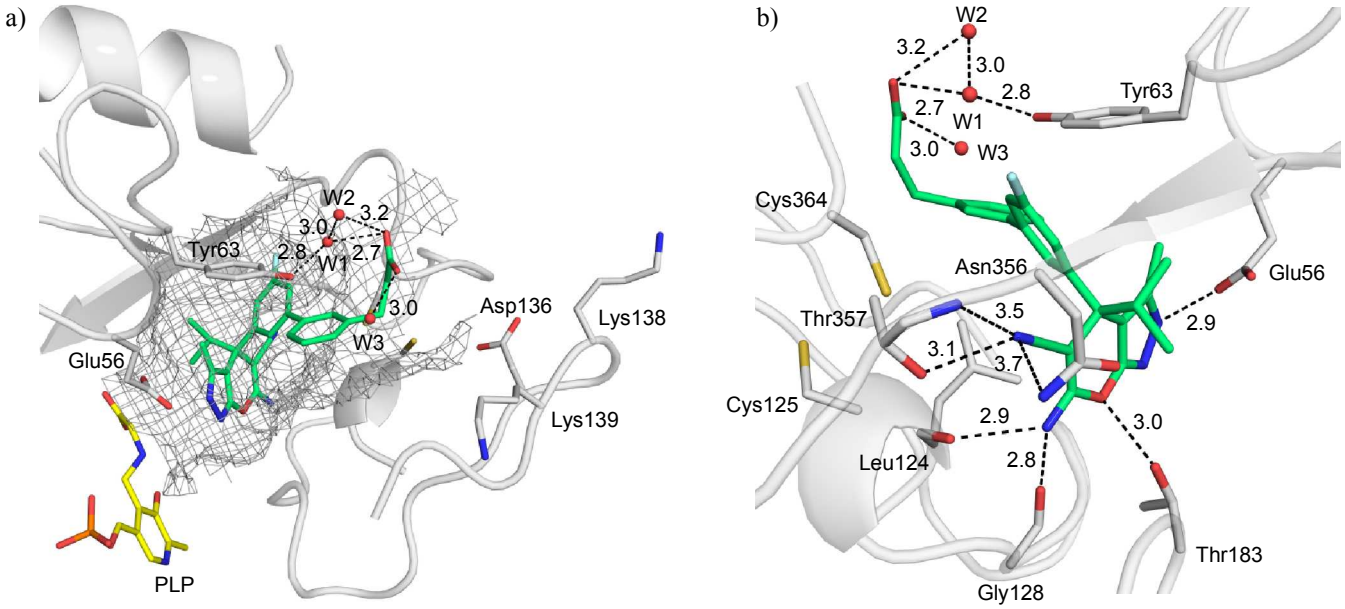

Binding Mode of (+)-85

Ligand (+)-**85** nicely occupies the substrate-binding site of *Pv*SHMT (Figure 3). As seen in all cocrystal structures reported herein and previously,[40] both active sites from the *Pv*SHMT homodimer are occupied by (+)-**85**. From the cocrystal structure, it can be derived that (+)-**85** (as well as the other pyrazolopyran ligands) is (*R*)-configured at the stereogenic center. The overall binding mode matches well the one from a *N*-formyl-THF derivative (Figure 4) in *Pv*SHMT

(PDB Code: 4OYT, 2.4 Å).[36] The cysteine bridge formed by Cys125 and Cys364 is found in its reduced form. The pyrazolopyran core is deeply buried into the pteridine pocket and is in close proximity to the cofactor PLP (Figure 3a). The core is anchored into the active site *via* a strong H-bond network, establishing an array of polar interactions similar to the ones seen in the two previously obtained cocrystal structures (Figure 3b).[40] The N(2) atom of the pyrazole ring is protonated and forms a short ionic H-bond with the side chain of Glu56. The protonation of N(2) is also seen in the unbound ligand state, as evidenced by the three small-molecule X-ray crystal structures recorded for (±)-**4**, (±)-**70**, and (±)-**88** (SI, Section S4.4, the structure of (±)-**88** is shown there). N(2)-protonation is supported by both the bond length in the pyrazole ring as well as by H-bonding interactions between neighboring molecules in the crystal lattice (SI, Section 4.4.2, Figure S28).

The biaryl moiety is located in the *p*ABA channel and directs the carboxylate side chain towards the periphery of the protein where Tyr63 adopts a conserved position in all structures (Figure 3a). We had hypothesized that extension of the carboxylate chain in (+)-**85** might allow interaction with Lys138 or Lys139 *via* a salt-bridge, consequently improving the binding affinity. This interaction was suggested by molecular dynamics simulation where Lys139 was found to be able to swing towards the ligand (SI, Section S5, Figure S30). However, this was not observed in the cocrystals with either (+)-**85**, or with (+)-**80** or (+)-**81** (Figure 3a and SI, Section S4.3, Figures S20 and S21). The carboxylate of (+)-**85** in a gauche conformation of the side chain is actually engaged in a water-mediated interaction with Tyr63 *via* W1 ($d(O^{-}\cdots O_{W1})$ = 2.7 Å and $d(O_{W1}\cdots O_{Tyr})$ = 2.8 Å). Two additional water molecules (W2 and W3) participate in solvating the carboxylate; no other protein residues are in their close proximity. Various short apolar protein-ligand contacts are depicted in the SI, Section 4.3, Figure S19. The isopropyl and methyl

groups attached to the core provide an optimal filling of small lipophilic pockets. The *meta*-fluorine atom is involved into hydrophobic contacts with Lys355 and Pro367.

Binding Modes of (+)-80 and (+)-81

Ligands (+)-**80** and (+)-**81** display a very similar binding mode to (+)-**85** in complex with *Pv*SHMT (SI, Section S4.3, Figure S20 and S21). For those two inhibitors the water-mediated interaction with Tyr63 is not observed, the carboxylates of (+)-**80** and (+)-**81** being at a distance of 3.9 and 4.4 Å from the OH group of Tyr63, respectively. In the complex of (+)-**81** with *Pv*SHMT complex, one water molecule (W1) could be resolved in close distance to the carboxylate of the ligand (d(C=O···W1) = 2.9 Å), but it is too far away from Tyr63 or any other residue to form a second bridging H–bond. The pyrazolopyran core maintains the key interactions seen in the complex of (+)-**85** (SI, Section S4.3, Figure S21). Noticeably, in the cocrystal structure with (+)-**80** two water molecules are found participating in the binding of the core (SI, Section S4.3, Figure S20a). A first water molecule (W1) is taking part to a tripod-shaped interaction, bridging the N(2) atom of the pyrazole ring with the side chains of Glu56 and His129. Additionally, the N(2) atom is at a short distance to Glu56. The second water molecule (W2) bridges the backbone C=O of Leu124 and the side chain of Thr357 *via* two hydrogen bonds, and is at van der Waals distance to the nonbasic NH_2 moiety (3.1 Å). However, analysis of the bond angles suggests more favorable interactions of the core NH_2 group with the backbone C=O of Leu124 and Gly128 than with W2.

The CF_3 moiety in (+)-**80** and (+)-**81** nicely fills the small lateral pocket, participating in short dipolar C–F···H–C and C–F···C=O interactions.[55–57] This is highlighted in the cocrystal structure with (+)-**80**, in which one of the C–F bonds is nearly orthogonal to the backbone C=O

of Lys355 (d(F···C) = 3.4 Å, angle F···C=O = 71°) (SI, Section S4.3, Figure S20b). While a second C–F bond interacts closely with Lys355 *via* a $F\cdots NH^+$ interaction ($d(F\cdots NH^+)$ = 3.4 Å). Interestingly, in the complex (+)-**81**-*Pv*SHMT, Cys364 points towards the CF_3 moiety at a S···F distance of 2.9 Å (SI, Section S4.3, Figure S21b) possibly forming a weak H-bond type interaction.[58]

Spatial Location of the Carboxylate Moiety in the Complexes of (+)-81 and (+)-85

Figure 4 shows an overlay of ligands (+)-**81** and (+)-**85** with a *N*-formyl-THF substrate previously cocrystallized with *Pv*SHMT (PDB Code: 4OYT, 2.4 Å).[36] Superimposition shows a good match between the pyrazolopyran ligands and *N*-formyl-THF (Figure 4).

Figure 4. a) Overlay of (+)-**81** (from PDB ID: 5GVM, 2.3 Å), (+)-**85** (from PDB ID: 5GVN, 2.3 Å), and *N*-formyl-THF (from PDB ID: 4OYT, 2.4 Å) in *Pv*SHMT (protein coordinates taken from PDB ID: 5GVN, 2.3 Å) confirms the similar positions of the carboxylate moieties of (+)-**81** and (+)-**85** to the glutamate side chain of THF. PLP is omitted for clarity. The water molecules (W1, W2, and W3 from the complex with (+)-**85**, and W4 from the complex with (+)-**81**) are represented as red spheres. Color code: $C_{protein}$ grey, C_{THF} yellow, $C_{(+)\text{-}\mathbf{81}}$ grey, $C_{(+)\text{-}\mathbf{85}}$ lime, F light cyan, N blue, O red, S yellow. b) Molecular structure of *N*-formyl-THF.

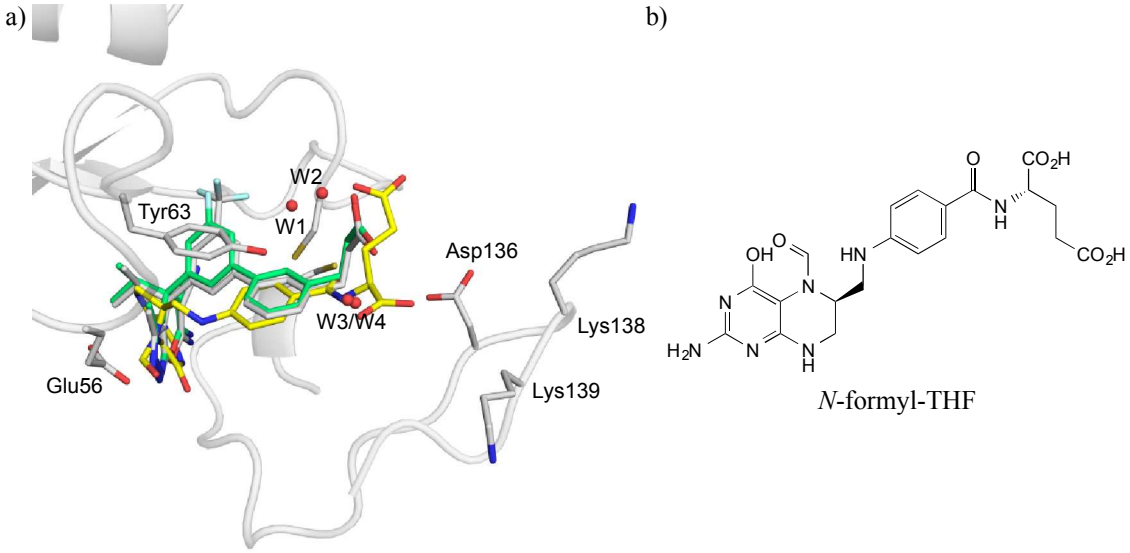

The position of the terminal phenyl ring of the two new ligands matches well with the *para*-aminobenzoyl side chain of the THF derivative. The carboxylate moiety of each inhibitor points upwards in the similar direction to the glutamate side chain of the natural substrate. Grafting the monoglutamate tail of THF onto our scaffold was not attempted as modeling suggested only a poor overlay with the corresponding amino acid of THF. Furthermore, we had previously installed this glutamate tail on a thiophene-based ligand, giving inhibition only in the micromolar IC_{50} range.[40]

Cys364–Loop Movement

The loop containing Cys364, named herein as Cys364-loop, is highly flexible as a consequence of its unique feature to exist either in a reduced or oxidized state in which a covalent disulfide bond between Cys125 and Cys364 is formed.[35] This flexibility is not limited to the plasmodial SHMT, but is also found in human SHMT despite its inability to form the disulfide bridge.[41] In

the cocrystals with (+)-**80**, (+)-**81**, or (+)-**85**, the location of the Cys364–loop differs markedly (Figure 5a).

Figure 5. a) Superimposition of the complexes of *Pv*SHMT with (+)-**80**, (+)-**81**, and (+)-**85**. b) Superimposition of the complexes with (+)-**1**, (+)-**4**, (+)-**7**, (+)-**80**, (+)-**81**, (+)-**85**, and (+)-**89** (the structure of (+)-**89** is shown in the SI, Section S4.3, Figure S23). Only ligand (+)-**85** is shown for clarity. The protein loops and β-strands are represented as cartoon; the active site surface is represented as grey mesh. PLP and water molecules omitted for clarity. Color code: $C_{(+)\text{-}\mathbf{1}\text{–}Pv\text{SHMT}}$ pink, $C_{(+)\text{-}\mathbf{4}\text{–}Pv\text{SHMT}}$ orange, $C_{(+)\text{-}\mathbf{7}\text{–}Pv\text{SHMT}}$ yellow, $C_{(+)\text{-}\mathbf{80}\text{–}Pv\text{SHMT}}$ marine-blue, $C_{(+)\text{-}\mathbf{81}\text{–}Pv\text{SHMT}}$ green, $C_{(+)\text{-}\mathbf{85}\text{–}Pv\text{SHMT}}$ grey, $C_{(+)\text{-}\mathbf{89}\text{–}Pv\text{SHMT}}$ cyan, $C_{(+)\text{-}\mathbf{80}}$ yellow, $C_{(+)\text{-}\mathbf{81}}$ grey, $C_{(+)\text{-}\mathbf{85}}$ lime, F light cyan, N blue, O red, S yellow.

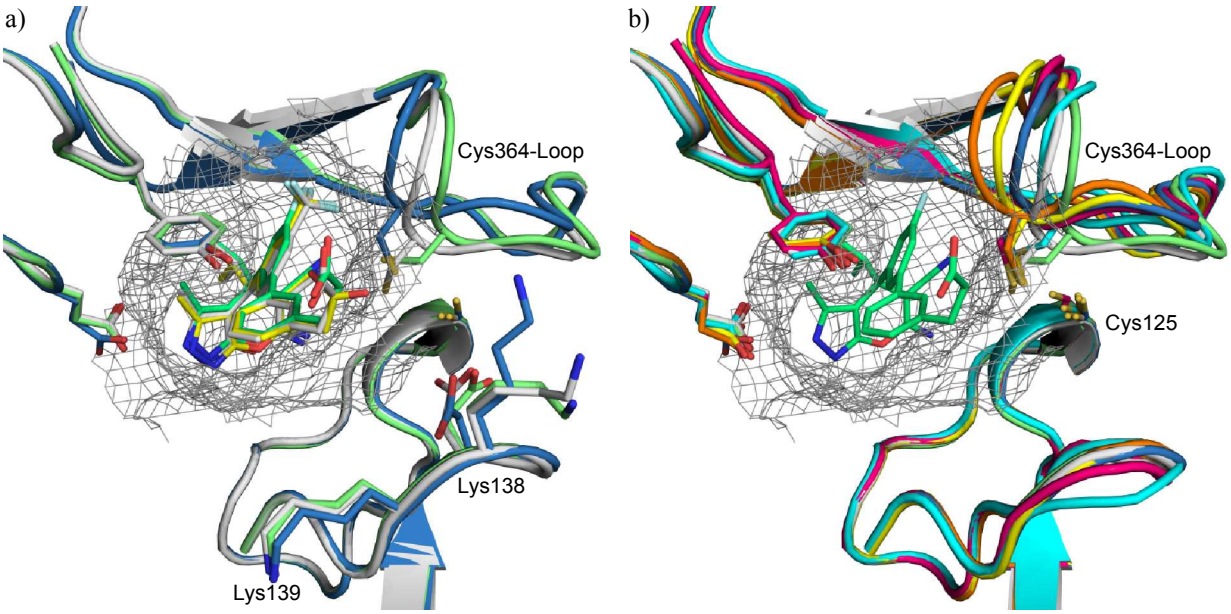

In comparison with the Cys364–loop from the (+)-**85**–*Pv*SHMT complex (grey), the Cys364–loop of the (+)-**80**–*Pv*SHMT complex (marine-blue) is moved towards the ligand, whereas in the *Pv*SHMT complex with CF_3-substitued (+)-**81** (green) the loop is pushed away, but unexpectedly

in this case to the opposite side (Figure 5a). This flexibility is well exemplified by the S–S distance between Cys125 and Cys364 which ranges from 2.9 to 4.0 Å across all structures.

The high degree of flexibility of the Cys364–loop is well exhibited by overlaying all five new cocrystal structures and the two previously reported ones (Figure 5b).[40] Although a trifluoromethyl group is sterically bigger than a cyano group, in the upper part of the pocket they both share a rather similar occupancy volume (SI, Section S4.3, Figure S24). This results in quasi-identical loops conformations with bound ligands (+)-**1** (pink) and (+)-**80** (marine-blue) (Figure 5b and SI, Section S4.3, Figure S22). In general, the Cys364–loop is located at comparable positions, independently of having a CN or CF_3 moiety as shown in the complexes with (+)-**1**, (+)-**4**, (+)-**7** and (+)-**80**. At the exception of the cocrystal with (+)-**89** (cyan, for structure of (+)-**89** see SI, Section S4.3, Figure S23), where the loop shifts to the right as in the structure with (+)-**81** (green) (Figure 5b and SI, Section S4.3, Figure S23). Interestingly in both cases the Cys364 points towards the ligand and not to Cys125. This movement of the cysteine residue seems to be associated with the change in conformation, however, careful analysis of the structures and of the neighboring residues did not allow to rationally explain this observation yet.

To further study the loop conformation, molecular dynamics simulations were performed using the protein coordinates from 4PFF.[36] The full apo enzyme dimer was simulated in its reduced form without any ligand in the active site. The Cys364–loop displayed large fluctuation in contrary to the other loops, which occupy much more conserved positions (SI, Section S5, Figure S30). This is supported by the different conformations seen in the cocrystal structures. The flexibility of the Cys364–loop is not only specific to *Pv*SHMT; human SHMT1 and 2 also show a high degree of conformational flexibility in this loop, as recently demonstrated by Marani *et al.*[41]

CONCLUSIONS

An extended library of 77 pyrazolopyran-based inhibitors was designed based on X-ray cocrystal structure information, synthesized, and tested on targets *At*- and *Pf*SHMT, and *in vitro* on the sensitive strain *Pf*NF54. The EC_{50} values from the cell-based assay correlated particularly well with the IC_{50} values in the *At*SHMT assay. Similar trends were obtained in the *Pf*SHMT assay, although the absolute IC_{50} values were in less good agreement with the EC_{50} values. The *in vitro* results were therefore used for lead optimization through structure-based design. The major aim of this new study was to improve metabolic stability as an important property of the ligands while maintaining high binding affinity and low cytotoxicity, which were properties already achieved by the earlier ligand series.[40] In each of the new ligand series prepared, ligands with low to single-digit nanomolar EC_{50} values were identified. The pyrazolopyran core was maintained in all ligands. Its substitution with methyl and isopropyl groups at the pyrazole ring and the stereogenic center, respectively, proved to be optimal. Introduction of a *meta*-CF_3 or *meta*-F substituent into the phenyl ring departing from the stereogenic center greatly enhanced target and *in vitro* potency. The terminal thiophene ring in the initial hit series[40] could be substituted by saturated *N*-heterocycles, while maintaining high potency. Substitution by aromatic *N*-heterocyclic analogues, such as a pyridyl group, afforded ligands with high *in vitro* antiparasitic efficacy in the single digit nanomolar range (e.g. (±)-**61**: EC_{50} = 3.2 nM). However, these strongly-binding compounds showed unsatisfactory metabolic stability. The desired stability at high target and *in vitro* affinity and low cytotoxicity was finally reached with a series of compounds featuring a carboxylic acid side chain of different lengths, departing from a terminal aryl or piperidine rings and reaching to the periphery of the protein. The most

interesting of these carboxylates showed an improved half-life in human liver microsomes ($t_{1/2}$ > 2 h), high *in vitro* activities (EC_{50} = 10–19 nM), and no cytotoxicity, neither hERG inhibition nor mutagenicity was observed. Given the early stage of the project, metabolism *via* non-microsomal enzymes was not explored and the potential for other routes of metabolism (*e.g.* phase II conjugation) cannot be ruled out at this stage. Chiral recognition at the active site is effective, and a large difference in activity between enantiomers of an optically resolved ligand was observed. Gratifyingly, the enantiopure ligand (+)-**86** also showed an improved microsomal half-life. The promising candidate (+)-**86** displayed a significant *in vivo* efficacy, at 4 × 50 mg/kg (p.o.) in a *Pf*SCID mouse model, with a reduction of 73% of parasitemia compared to untreated mice. Hence, validating SHMT as a viable *in vivo* antimalarial target. This outcome encourages us to further develop SHMT inhibitors and their pharmacokinetic properties in the perspective to reach complete clearance of parasitemia. A series of 5 new cocrystal structures showed the good fit of the ligands with the bound substrate THF; the pyrazolopyran core occupying the pteridine pocket, the substituted phenyl ring at the stereogenic center fills the *p*ABA channel, and the terminal carboxylate side chains mimic the terminal glutamate side chain of the substrate. A small water cluster solvating the carboxylate of (+)-**85** and establishing a water-mediated H-bonding interaction to Tyr63 was observed for the first time. In addition, the high degree of flexibility of the Cys364–loop was demonstrated by the overlay of 7 cocrystal structures. All this new structural information will be highly valuable for future development of inhibitors of SHMT, which in the meantime is not only a new antimalarial target but also raises interest as a new anticancer target.[41,43,59]

EXPERIMENTAL SECTION

Chemical Synthesis. Only the synthesis and characterization of selected final compounds ((±)-**20**, (±)-**33**, (±)-**61** and (±)-**80**–**87**) are described herein, together with general procedures. Synthesis and characterization of intermediates towards (±)-**86** are described herein (according to Scheme 6). Purity of all final compounds was determined to be ≥95% by elemental analysis and/or by analytical high pressure liquid chromatography (HPLC) (for the HPLC conditions see SI, Section S1.1). More information about the materials, synthesis of intermediates, and characterization can be found in the SI, Section S1.

Scheme 6. a) Synthesis of the piperidine building block **90** from commercially available *N*-Boc protected acetic acid **91** *via* **92**. b) Synthesis of ligands (±)-**86**, (+)-**86**, and (–)-**86** by first coupling the building block **38** with **90**, then Knoevenagel condensation with ketone **93** leading to the dinitrile **94**, and formation of the pyrazolopyran core (±)-**95**.[a]

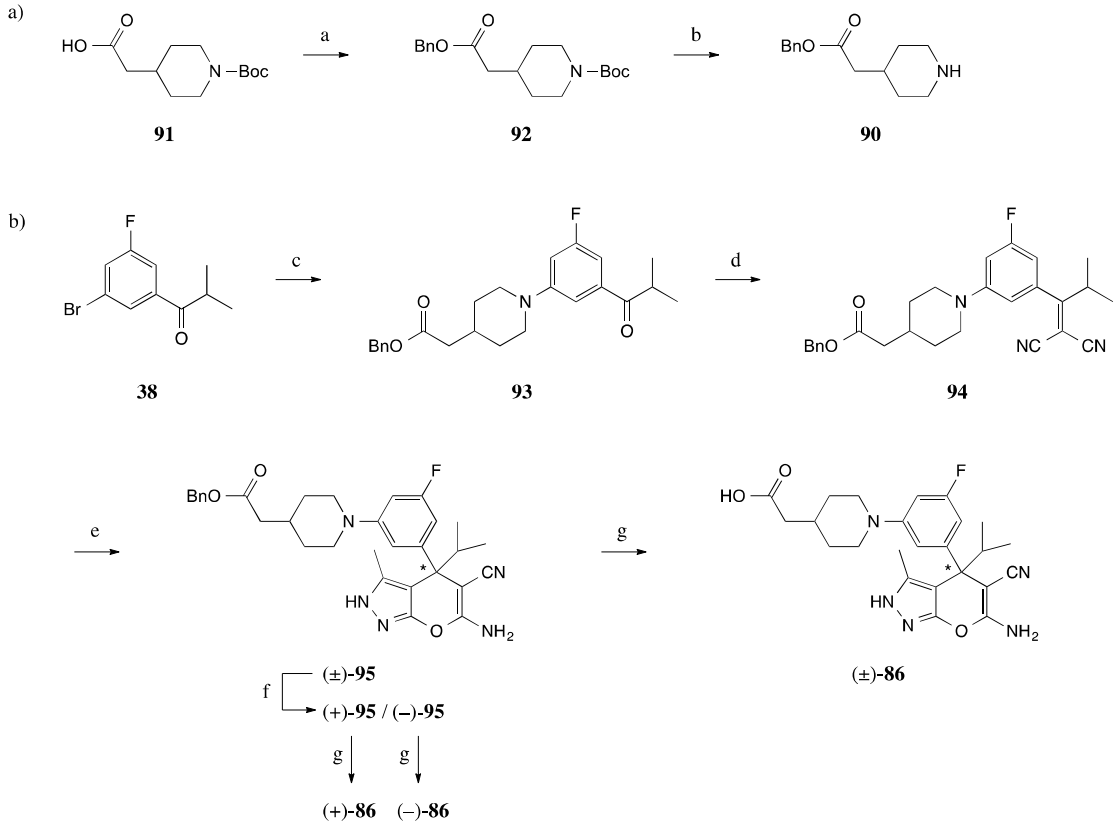

[a]Reagents and conditions: (a) benzyl bromide, K_2CO_3, acetone, reflux, 16 h, quant.; (b) TFA, CH_2Cl_2, 23 °C, 16 h, 94%; (c) **90**, Cs_2CO_3, $[Pd_2(dba)_3]$ (2.0 mol %), X-Phos (8.0 mol %), 1,4-dioxane, 110 °C, 16 h, 94%; (d) malononitrile, $TiCl_4$, pyridine, $CHCl_3$, 63 °C, 60 h, 77%; (e) 3-methyl-2-pyrazolin-1-one, piperidine, 1,4-dioxane/BnOH 1:1, μw, 65 °C, 2 h, 25%; (f) separation of the enantiomers of (±)-**95** by chiral-phase HPLC (column, Daicel, Chiralpak-IA 250 mm × 20 mm; flow, 15 mL/min; detection, 254 nm; eluent, hexane/EtOAc/*i*PrOH 60:30:10); (g) H_2, 10% [Pd/C], MeOH, 23 °C, 16 h, 94–100%.

General Procedure GP1 for the Synthesis of the Pyrazolopyran Core (According to Scheme 1). Distilled solvents were used and the reaction was carried out under Ar atmosphere. A mixture of the dinitrile (0.331 mmol, 1.0 eq.) and the corresponding pyrazolone (0.364 mmol, 1.1 eq.) was suspended in a mixture of ethanol/1,4-dioxane 1:1 (0.80 mL) (in case of benzyl protected analogues, benzyl alcohol was used instead of ethanol to prevent transesterification). Addition of distilled piperidine (3.31 mmol, 10.0 eq.) led to an orange solution. The mixture was stirred at 65 °C for 3.5 h in a microwave oven, diluted with water (10 mL) and EtOAc (10 mL). The layers were separated, and the aqueous layer was extracted three times with EtOAc (3 × 10 mL). The combined organic layers were washed with brine, dried over Na_2SO_4, filtered, and evaporated to afford the crude pyrazolopyran.

General Procedure GP2 for the Benzyl Deprotection (According to Scheme 6). A solution of the benzyl ester (0.175 mmol, 1.0 eq.) in MeOH (2.0 mL) was treated with 10% [Pd/C] (0.047 mmol, 0.27 eq.), H_2 was bubbled through the solution for 10 min. The mixture was stirred at 23 °C for 16 h and filtered through a PTFE microfilter (45/25). The mother liquor was evaporated to afford the carboxylic acid.

(±)-5-{3-[6-Amino-5-cyano-3-methyl-4-isopropyl-2,4-dihydropyrano[2,3-*c*]pyrazol-4-yl]-5-(trifluoromethyl)phenyl}-*N*,*N*-dimethylthiophene-2-sulfonamide ((±)-20). Following general procedure **GP1**, column chromatography (SiO_2; cyclohexane/EtOAc 70:30 → 50:50) and recrystallization from CH_2Cl_2/hexane gave (±)-**20** (65 mg, 27%) as a white solid. R_f = 0.14 (SiO_2; cyclohexane/EtOAc 50:50); m.p. 155–158 °C; ^{1}H NMR (400 MHz, THF-d_8): δ = 0.88

and 0.97 (d, J = 6.6 Hz, 6 H; CHMe_2), 1.86 (s, 3 H; Me), 2.73 (s, 6 H; NMe_2), 2.89 (sept., J = 6.6 Hz, 1 H; CHMe$_2$), 6.30 (br. s, 2 H; NH_2), 7.53 (d, J = 3.9 Hz, 1 H; H–C(3)), 7.58 (d, J = 3.9 Hz, 1 H; H–C(4)), 7.67 (br. s, 1 H; H–C(6')), 7.86 (br. s, 1 H; H–C(4')), 7.93 (br. s, 1 H; H–C(2')), 11.36 ppm (br. s, 1 H; NH); ^{13}C NMR (101 MHz, THF-d_8): δ = 12.17 (Me), 18.68 and 19.20 (CHMe_2), 36.36 (CHMe$_2$), 38.11 (NMe_2), 48.83 (C(4")), 62.76 (C(5")), 99.35 (C(3a")), 119.94 (CN), 121.72 (q, ^3J(C, F) = 3.8 Hz; C(4')), 125.12 (q, ^1J(C, F) = 272.4 Hz; CF_3), 125.86 (C(4)), 126.27 (q, ^3J(C, F) = 3.8 Hz; C(6')), 130.55 (C(2')), 131.90 (q, ^2J(C, F) = 31.8 Hz; C(5')), 134.01 (C(3)), 134.66 (C(1')), 135.76 (C(3")), 136.82 (C(5)), 148.12 (C(3')), 149.60 (C(2)), 157.43 (C(7a")), 162.75 ppm (C(6")); ^{19}F NMR (377 MHz, THF-d_8): δ = –63.42 ppm (s; CF_3); IR (ATR): $\tilde{\nu}$ = 3427 (w), 3336 (w), 3217 (w), 2963 (w), 2192 (m), 1644 (s), 1604 (s), 1588 (m), 1487 (m), 1460 (w), 1427 (w), 1398 (s), 1384 (w), 1308 (m), 1272 (w), 1239 (w), 1159 (s), 1128 (s), 1099 (w), 1048 (m), 1009 (w), 958 (m), 919 (w), 897 (w), 812 (w), 724 (w), 709 (s), 692 (w), 659 cm^{-1} (m); HR-ESI-MS: m/z (%): 569.1611 (100, $[M + NH_4]^+$, calcd for $C_{24}H_{28}F_3N_6O_3S_2^+$: 569.1611), 552.1343 (15, $[M + H]^+$, calcd for $C_{24}H_{25}F_3N_5O_3S_2^+$: 552.1345); elemental analysis calcd (%) for $C_{24}H_{24}F_3N_5O_3S_2$ (551.6): C 52.26, H 4.39, N 12.70, F 10.33, S 11.63; found: C 52.25, H 4.32, N 12.66, F 10.23, S 11.49.

(±)-6-Amino-4-[3-(4,4-difluoropiperidin-1-yl)-5-(trifluoromethyl)phenyl]-3-methyl-4-isopropyl-2,4-dihydropyrano[2,3-*c*]pyrazole-5-carbonitrile ((±)-33). Following general procedure **GP1**, column chromatography (SiO_2; cyclohexane/EtOAc 80:20 → 60:40) and recrystallization from CH_2Cl_2/hexane gave (±)-**33** (118 mg, 38%) as a white solid. R_f = 0.16 (SiO_2; cyclohexane/EtOAc 60:40); m.p. 250 °C (decomp.); ^{1}H NMR (400 MHz, THF-d_8): δ = 0.84 and 0.93 (d, J = 6.6 Hz, 6 H; CHMe_2), 1.85 (s, 3 H; Me), 1.96–2.16 (m, 4 H; H-C(3", 5")), 2.81 (sept., J = 6.6 Hz, 1 H; CHMe$_2$), 3.30–3.48 (m, 4 H; H–C(2", 6")), 6.17 (br. s, 2 H; NH_2),

7.03–7.16 (m, 2 H; H–C(4', 6')), 7.28 (br. t, J = 2.0 Hz, 1 H; H–C(2')), 11.27 ppm (br. s, 1 H; NH); ^{13}C NMR (101 MHz, THF-d_8): δ = 12.27 (Me), 18.75 and 19.26 (CHMe_2), 34.30 (t, ^2J(C, F) = 22.9 Hz; C(3", 5")), 36.44 (CHMe$_2$), 47.28 (t, ^3J(C, F) = 5.3 Hz; C(2", 6")), 48.82 (C(4)), 63.31 (C(5)), 99.73 (C(3a)), 111.68 (q, ^3J(C, F) = 3.8 Hz; C(4')), 117.08 (q, ^3J(C, F) = 3.9 Hz; C(6')), 120.19 (CN), 121.43 (d, ^5J(C, F) = 1.7 Hz; C(2')), 122.79 (t, ^1J(C, F) = 241.2 Hz; C(4")), 125.64 (q, ^1J(C, F) = 272.3 Hz; CF_3), 131.43 (q, ^2J(C, F) = 31.2 Hz; C(5')), 135.70 (C(3)), 147.32 (C(1')), 151.62 (C(3')), 157.43 (C(7a)), 162.51 ppm (C(6)); ^{19}F NMR (377 MHz, THF-d_8): δ = –98.37 (quint., ^3J(H, F) = 13.8 Hz; CF_2), –63.25 ppm (s; CF_3); IR (ATR): $\tilde{\nu}$ = 3505 (w), 3401 (w), 3243 (m), 2965 (w), 2838 (w), 2199 (s), 1635 (s), 1606 (w), 1595 (w), 1584 (m), 1483 (w), 1466 (m), 1392 (m), 1379 (m), 1365 (s), 1306 (s), 1278 (w), 1234 (m), 1180 (w), 1171 (w), 1156 (m), 1133 (w), 1115 (m), 1097 (s), 1053 (s), 1020 (w), 995 (w), 984 (m), 958 (w), 946 (w), 931 (w), 892 (w), 863 (s), 814 (w), 793 (w), 742 (s), 707 (m), 689 (m), 647 cm^{-1} (w); HR-ESI-MS: *m/z* (%): 482.1970 (100, $[M + H]^+$, calcd for $C_{23}H_{25}F_5N_5O^+$: 482.1974); analyt. HPLC: t_R = 14.23 min (purity > 99%; method B).

(±)-6-Amino-3-methyl-4-isopropyl-4-[3-(pyridin-4-yl)-5-(trifluoromethyl)phenyl]-2,4-dihydropyrano[2,3-*c*]pyrazole-5-carbonitrile ((±)-61). Following general procedure **GP1**, column chromatography (SiO_2; cyclohexane/EtOAc 60:40 → 10:90) and recrystallization from CH_2Cl_2/hexane gave (±)-**61** (115 mg, 36%) as a white solid. R_f = 0.10 (SiO_2; cyclohexane/EtOAc 20:80); m.p. 244–246 °C; ^{1}H NMR (400 MHz, THF-d_8): δ = 0.88 and 0.98 (d, J = 6.6 Hz, 6 H; CHMe_2), 1.86 (s, 3 H; Me), 2.93 (sept., J = 6.6 Hz, 1 H; CHMe$_2$), 6.29 (br. s, 2 H; NH_2), 7.54–7.63 (m, 2 H; H–C(3", 5")), 7.71 (br. s, 1 H; H–C(6')), 7.88 (br. s, 1 H; H–C(4')), 7.99 (br. s, 1 H; H–C(2')), 8.58–8.67 (m, 2 H; H–C(2", 6")), 11.37 ppm (br. s, 1 H; NH); ^{13}C NMR (101 MHz, THF-d_8): δ = 12.22 (Me), 18.69 and 19.23 (CHMe_2), 36.43 (CHMe$_2$), 48.93 (C(4)), 62.96 (C(5)),

99.39 (C(3a)), 120.14 (CN), 122.39 (C(3", 5")), 122.73 (q, ^3J(C, F) = 3.8 Hz; C(4'))), 123.33 (q, ^1J(C, F) = 272.4 Hz; CF_3), 126.34 (q, ^3J(C, F) = 3.7 Hz; C(6')), 131.72 (q, ^2J(C, F) = 32.0 Hz; C(5')), 131.62 (C(2')), 135.73 (C(3)), 140.19 (C(4")), 147.53 (C(3')), 147.71 (C(1')), 151.37 (C(2", 6")), 157.45 (C(7a)), 162.68 ppm (C(6)); ^{19}F NMR (377 MHz, THF-d_8): δ = –63.22 ppm (s; CF_3); IR (ATR): $\tilde{\nu}$ = 3470 (w), 3260 (m), 3082 (w), 2975 (w), 2192 (s), 1639 (s), 1606 (s), 1592 (s), 1553 (w), 1515 (w), 1487 (m), 1455 (w), 1390 (s), 1378 (w), 1341 (m), 1325 (w), 1268 (s), 1221 (w), 1185 (w), 1158 (m), 1118 (s), 1102 (s), 1080 (m), 1070 (w), 1054 (m), 996 (w), 984 (w), 962 (w), 925 (w), 901 (m), 883 (w), 869 (w), 824 (s), 794 (m), 752 (w), 731 (w), 719 (w), 709 (m), 690 (m), 673 (w), 644 (w), 626 (m), 606 cm^{-1} (w); HR-ESI-MS: *m/z* (%): 440.1694 (100, $[M + H]^+$, calcd for $C_{23}H_{21}F_3N_5O^+$: 440.1693); elemental analysis calcd (%) for $C_{23}H_{20}F_3N_5O$ (439.4): C 62.86, H 4.59, N 15.94, F 12.97; found: C 62.78, H 4.52, N 16.01, F 13.06.

(±)-{3'-[6-Amino-5-cyano-3-methyl-4-isopropyl-2,4-dihydropyrano[2,3-*c*]pyrazol-4-yl]-5'-(trifluoromethyl)[1,1'-biphenyl]-3-yl}acetic Acid ((±)-80). Following general procedure **GP2**, (±)-**80** (240 mg, 95%) was obtained as a white solid. R_f = 0.29 (SiO_2; cyclohexane/EtOAc/Formic acid 40:60:01); m.p. 154–157 °C; ^{1}H NMR (400 MHz, CD_3OD): δ = 0.91 and 1.03 (d, *J* = 6.6 Hz, 6 H; CH*Me*$_2$), 1.85 (s, 3 H; Me), 2.93 (sept., *J* = 6.6 Hz, 1 H; C*H*Me$_2$), 3.70 (d, *J* = 1.0 Hz, 2 H; C*H*$_2$COOH), 7.34 (dt, *J* = 7.5, 1.5 Hz, 1 H; H–C(4)), 7.44 (t, *J* = 7.6 Hz, 1 H; H–C(5)), 7.48–7.53 (m, 1 H; H–C(6)), 7.53–7.57 (m, 1 H; H–C(2)), 7.60 (br. s, 1 H; H–C(4')), 7.77 (br. s, 1 H; H–C(6')), 7.88 ppm (br. s, 1 H; H–C(2')); ^{13}C NMR (101 MHz, CD_3OD): δ = 11.93 (Me), 18.76 and 19.25 (CH*Me*$_2$), 36.69 (*C*HMe$_2$), 41.92 (*C*H$_2$COOH), 62.28 (C(5")), 100.72 (C(3a")), 121.70 (CN), 123.05 (q, ^3J(C, F) = 3.6 Hz; C(6')), 125.24 (q, ^3J(C, F) = 3.7 Hz; C(4')), 125.69 (q, ^1J(C, F) = 271.8 Hz; CF_3), 126.83 (C(6)), 129.32 (C(2)), 130.28 and

130.30 (C(4, 5)), 131.63–132.26 (m, 2 C; C(2', 5')), 137.20 (C(3)), 137.58 (C(3")), 141.30 (C(1')), 143.39 (C(1)), 147.36 (C(3')), 157.54 (C(7a")), 163.93 (C(6")), 175.61 ppm (C=O), C(4") hidden under the residual solvent peak; ^{19}F NMR (377 MHz, CD_3OD): δ = –63.99 ppm (s; CF_3); IR (ATR): $\tilde{\nu}$ = 3317 (br. w), 2970 (w), 2189 (m), 1712 (m), 1633 (s), 1586 (s), 1488 (w), 1448 (w), 1388 (s), 1351 (m), 1268 (m), 1155 (w), 1121 (s), 1078 (w), 1043 (w), 892 (w), 786 (m), 747 (w), 704 cm^{-1} (m); HR-ESI-MS: *m/z* (%): 497.1790 (100, $[M + H]^+$, calcd for $C_{26}H_{24}F_3N_4O_3^+$: 497.1795); analyt. HPLC: t_R = 14.46 min (purity = 97%; method A).

(±)-3-{3'-[6-Amino-5-cyano-3-methyl-4-isopropyl-2,4-dihydropyrano[2,3-*c*]pyrazol-4-yl]-5'-(trifluoromethyl)[1,1'-biphenyl]-3-yl}propanoic Acid ((±)-81). Following general procedure **GP2**, (±)-**81** (170 mg, 94%) was obtained as a white solid. R_f = 0.38 (SiO_2; cyclohexane/EtOAc/Formic acid 40:60:01); m.p. 138–140 °C; ^{1}H NMR (400 MHz, CD_3OD): δ = 0.91 and 1.03 (d, *J* = 6.5 Hz, 6 H; CH*Me*$_2$), 1.85 (s, 3 H; Me), 2.66 (t, *J* = 7.5 Hz, 2 H; CH_2CH_2COOH), 2.92 (sept., *J* = 6.6 Hz, 1 H; C*H*Me$_2$), 3.00 (t, *J* = 7.6 Hz, 2 H; CH_2CH_2COOH), 7.29 (dt, *J* = 7.2, 1.7 Hz, 1 H; H–C(4)), 7.36–7.46 (m, 2 H; H–C(5, 6)), 7.48 (t, *J* = 1.7 Hz, 1 H; H–C(2)), 7.59 (br. s, 1 H; H–C(4')), 7.75 (br. s, 1 H; H–C(6')), 7.86 ppm (br. t, *J* = 1.7 Hz, 1 H; H–C(2')); ^{13}C NMR (101 MHz, CD_3OD): δ = 11.95 (Me), 18.76 and 19.26 (CH*Me*$_2$), 32.00 (CH_2CH_2C=O), 36.69 (CH_2CH_2C=O), 36.71 (*C*HMe$_2$), 62.31 (C(5")), 100.71 (C(3a")), 121.72 (CN), 123.01 (q, ^3J(C, F) = 3.8 Hz; C(6')), 125.14 (q, ^3J(C, F) = 4.0 Hz; C(4')), 125.70 (q, ^1J(C, F) = 272.3 Hz; CF_3), 126.16 (C(6)), 128.28 (C(2)), 129.28 (C(4)), 130.31 (C(5)), 131.92 (q, ^5J(C, F) = 1.4 Hz; C(2')), 132.08 (q, ^2J(C, F) = 31.8 Hz; C(5')), 137.58 (C(3")), 141.26 (C(1')), 143.29 (C(3)), 143.59 (C(1)), 147.29 (C(3')), 157.54 (C(7a")), 163.92 (C(6")), 176.75 ppm (C=O), C(4") hidden under the residual solvent peak; ^{19}F NMR (377 MHz, CD_3OD): δ = –63.98 ppm (s; CF_3); IR (ATR): $\tilde{\nu}$ = 3313 (w), 2970 (w), 2189 (m), 1710 (m), 1633

(s), 1586 (s), 1488 (m), 1448 (w), 1388 (s), 1351 (m), 1268 (m), 1155 (m), 1121 (s), 1077 (w), 1042 (w), 887 (w), 865 (w), 793 (m), 736 (w), 705 (m), 632 cm^{-1} (w); HR-ESI-MS: *m/z* (%): 511.1948 (100, $[M + H]^+$, calcd for $C_{27}H_{26}F_3N_4O_3^+$: 511.1952); analyt. HPLC: t_R = 15.32 min (purity = 97%; method A).

(±)-(1-{3-[6-Amino-5-cyano-3-methyl-4-isopropyl-2,4-dihydropyrano[2,3-*c*]pyrazol-4-yl]-5-(trifluoromethyl)phenyl}piperidin-4-yl)acetic Acid ((±)-82). Following general procedure **GP2**, (±)-**82** (156 mg, 97%) was obtained as a white solid. R_f = 0.25 (SiO_2; cyclohexane/EtOAc/Formic acid 40:60:01); m.p. 238 °C (decomp.); ^{1}H NMR (400 MHz, CD_3OD): δ = 0.87 and 0.99 (d, J = 6.6 Hz, 6 H; CH*Me*$_2$), 1.31–1.51 (m, 2 H; H_{ax}–C(3, 5)), 1.82 (s, 3 H; Me), 1.83–2.01 (m, 3 H; H–C(3_{eq}, 4, 5_{eq})), 2.27 (d, J = 6.9 Hz, 2 H; C*H*$_2$COOH), 2.69–2.89 (m, 3 H; H_{ax}–C(2, 6) and C*H*Me$_2$), 3.59–3.78 (m, 2 H; H_{eq}–C(2, 6)), 7.03–7.08 (m, 2 H; H–C(4', 6')), 7.20 ppm (br. t, J = 2.0 Hz, 1 H; H–C(2')); ^{13}C NMR (101 MHz, CD_3OD): δ = 11.89 (Me), 18.81 and 19.28 (CH*Me*$_2$), 32.73 (C(3, 5)), 34.03 (C(4)), 36.66 (*C*HMe$_2$), 41.81 (*C*H$_2$COOH), 50.77 and 50.82 (C(2, 6)), 62.47 (C(5")), 101.09 (C(3a")), 112.05 (q, ^3J(C, F) = 4.0 Hz; C(6')), 116.81 (d, ^3J(C, F) = 4.6 Hz; C(4')), 121.73 (C(2')), 121.76 (CN), 125.92 (q, ^1J(C, F) = 271.8 Hz; CF_3), 131.98 (q, ^2J(C, F) = 31.3 Hz; C(5')), 137.57 (C(3")), 147.28 (C(3')), 153.46 (C(1')), 157.48 (C(7a")), 163.83 (C(6")), 176.34 ppm (C=O), C(4") hidden under the residual solvent peak; ^{19}F NMR (377 MHz, CD_3OD): δ = –64.11 ppm (s; CF_3); IR (ATR): $\tilde{\nu}$ = 3208 (w), 2931 (w), 2198 (m), 1708 (m), 1641 (s), 1598 (s), 1490 (w), 1462 (w), 1375 (s), 1325 (w), 1300 (s), 1263 (w), 1234 (w), 1156 (s), 1117 (s), 1058 (w), 993 (w), 950 (m), 910 (w), 875 (w), 854 (w), 805 (w), 790 (w), 746 (m), 703 (w), 686 cm^{-1} (m); HR-ESI-MS: *m/z* (%): 504.2215 (100, $[M + H]^+$, calcd for $C_{25}H_{29}F_3N_5O_3^+$: 504.2217); analyt. HPLC: t_R = 13.00 min (purity > 99%; method A).

(±)-3-(1-{3-[6-Amino-5-cyano-3-methyl-4-isopropyl-2,4-dihydropyrano[2,3-*c*]pyrazol-4-yl]-5-(trifluoromethyl)phenyl}piperidin-4-yl)propanoic Acid ((±)-83). Following general procedure **GP2**, (±)-**83** (298 mg, 97%) was obtained as a white solid. R_f = 0.27 (SiO_2; cyclohexane/EtOAc/Formic acid 40:60:01); m.p. 145–148 °C; ^{1}H NMR (400 MHz, CD_3OD): δ = 0.87 and 0.99 (d, J = 6.6 Hz, 6 H; CH*Me*$_2$), 1.24–1.41 (m, 2 H; H_{ax}–C(3, 5)), 1.40–1.50 (m, 1 H; H–C(4)), 1.60 (q, J = 7.2 Hz, 2 H; C*H*$_2$CH$_2$COOH), 1.72–1.92 (m, 5 H; H_{eq}–C(3, 5) and Me), 2.35 (t, J = 7.6 Hz, 2 H; CH$_2$C*H*$_2$COOH), 2.64–2.89 (m, 3 H; H_{ax}–C(2, 6) and C*H*Me$_2$), 3.58–3.78 (m, 2 H; H_{eq}–C(2, 6)), 7.04 (br. t, J = 1.6 Hz, 1 H; H–C(4')), 7.06 (br. t, J = 1.8 Hz, 1 H; H–C(6')), 7.19 ppm (br. t, J = 2.0 Hz, 1 H; H–C(2')); ^{13}C NMR (101 MHz, CD_3OD): δ = 11.89 (Me), 18.82 and 19.28 (CH*Me*$_2$), 32.26 (CH$_2$*C*H$_2$COOH), 32.65 (*C*H$_2$CH$_2$COOH), 32.80 (C(3, 5)), 36.44 (C(4)), 36.66 (*C*HMe$_2$), 50.92 and 50.98 (C(2, 6)), 62.47 (C(5")), 101.11 (C(3a")), 112.01 (q, ^3J(C, F) = 4.0 Hz; C(6')), 116.72 (q, ^3J(C, F) = 4.6 Hz; C(4')), 121.73 (C(2')), 121.76 (CN), 125.93 (q, ^1J(C, F) = 271.8 Hz; CF_3), 131.96 (q, ^2J(C, F) = 31.3 Hz; C(5')), 137.57 (C(3")), 147.26 (C(3')), 153.52 (C(1')), 157.47 (C(7a")), 163.83 (C(6")), 177.62 ppm (C=O), C(4") hidden under the residual solvent peak; ^{19}F NMR (377 MHz, CD_3OD): δ = –64.10 ppm (s; CF_3); IR (ATR): $\tilde{\nu}$ = 3310 (br. m), 2928 (w), 2188 (m), 1709 (m), 1633 (s), 1595 (s), 1485 (m), 1384 (s), 1302 (m), 1245 (w), 1155 (m), 1116 (s), 1057 (w), 993 (w), 950 (w), 913 (w), 851 (w), 793 (w), 744 (w), 690 (m), 674 cm^{-1} (w); HR-ESI-MS: *m/z* (%): 518.2369 (100, $[M + H]^+$, calcd for $C_{26}H_{31}F_3N_5O_3^+$: 518.2374); analyt. HPLC: t_R = 14.19 min (purity = 99%; method A); elemental analysis calcd (%) for $C_{26}H_{30}F_3N_5O_3$ (517.5): C 60.34, H 5.84, N 13.53, F 11.01; found: C 60.14, H 5.92, N 13.71, F 11.00.

(±)-{3'-[6-Amino-5-cyano-3-methyl-4-isopropyl-2,4-dihydropyrano[2,3-*c*]pyrazol-4-yl]-5'-fluoro[1,1'-biphenyl]-3-yl}acetic Acid ((±)-84). Following general procedure **GP2**, (±)-**84**

(162 mg, 85%) was obtained as a white solid. R_f = 0.26 (SiO_2; cyclohexane/EtOAc/Formic acid 40:60:01); m.p. 151–153 °C; ^{1}H NMR (400 MHz, CD_3OD): δ = 0.91 and 1.03 (d, J = 6.6 Hz, 6 H; CH*Me*$_2$), 1.88 (s, 3 H; Me), 2.86 (sept., J = 6.7 Hz, 1 H; C*H*Me$_2$), 3.68 (s, 2 H; CH_2COOH), 7.02–7.14 (m, 1 H; H–C(4')), 7.24 (m, 1 H; H–C(6')), 7.30 (dt, J = 7.6, 1.5 Hz, 1 H; H–C(4)), 7.40 (t, J = 7.6 Hz, 1 H; H–C(5)), 7.43–7.48 (m, 2 H; H–C(6, 2')), 7.50 ppm (br. s, 1 H; H–C(2)); ^{13}C NMR (101 MHz, CD_3OD): δ = 11.96 (Me), 18.88 and 19.34 (CH*Me*$_2$), 36.71 (*C*HMe$_2$), 41.93 (*C*H_2COOH), 62.52 (C(5")), 101.06 (C(3a")), 113.05 (d, ^2J(C, F) = 22.6 Hz; C(6')), 115.50 (d, ^2J(C, F) = 23.2 Hz; C(4')), 121.85 (CN), 124.13 (d, ^4J(C, F) = 2.4 Hz; C(2')), 126.71 (C(6)), 129.19 (C(2)), 130.03 (C(4)), 130.12 (C(5)), 136.97 (C(3)), 137.65 (C(3")), 141.63 (d, ^4J(C, F) = 2.3 Hz; C(1)), 144.31 (d, ^3J(C, F) = 8.1 Hz; C(1')), 148.71 (d, ^3J(C, F) = 6.8 Hz; C(3')), 157.46 (C(7a")), 163.84 (C(6")), 164.57 (d, ^1J(C, F) = 243.9 Hz; C(5')), 175.59 ppm (C=O), C(4") hidden under the residual solvent peak; ^{19}F NMR (377 MHz, CD_3OD): δ = –115.05 ppm (t, ^3J(H, F) = 10.1 Hz; F); IR (ATR): $\tilde{\nu}$ = 3314 (w), 2969 (w), 2188 (m), 1712 (m), 1632 (s), 1583 (s), 1487 (m), 1438 (w), 1383 (s), 1317 (w), 1163 (m), 1042 (w), 940 (w), 863 (w), 837 (w), 787 (m), 746 (w), 700 cm^{-1} (m); HR-ESI-MS: *m/z* (%): 447.1826 (100, $[M + H]^+$, calcd for $C_{25}H_{24}FN_4O_3^+$: 447.1827); analyt. HPLC: t_R = 10.84 min (purity = 96%; method A).

(±)-3-{3'-[6-Amino-5-cyano-3-methyl-4-isopropyl-2,4-dihydropyrano[2,3-c]pyrazol-4-yl]-5'-fluoro[1,1'-biphenyl]-3-yl}propanoic Acid ((±)-85). Following general procedure **GP2**, (±)-**85** (295 mg, 98%) was obtained as a white solid. R_f = 0.33 (SiO_2; cyclohexane/EtOAc/Formic acid 40:60:01); m.p. 139–141 °C; ^{1}H NMR (400 MHz, CD_3OD): δ = 0.91 and 1.03 (d, J = 6.6 Hz, 6 H; CH*Me*$_2$), 1.88 (s, 3 H; Me), 2.65 (t, J = 7.6 Hz, 2 H; CH_2CH_2COOH), 2.86 (sept., J = 6.7 Hz, 1 H; C*H*Me$_2$), 2.98 (t, J = 7.6 Hz, 2 H; CH_2CH_2COOH), 7.07 (ddd, ^3J(H, F) = 10.6 Hz, J = 2.4, 1.6 Hz, 1 H; H–C(4')), 7.18–7.30 (m, 2 H; H–C(4, 6')), 7.32–7.42 (m, 2 H; H–C(5, 6)), 7.42–

7.47 ppm (m, 2 H; H–C(2, 2')); ^{13}C NMR (101 MHz, CD_3OD): δ = 11.98 (Me), 18.87 and 19.35 (CH*Me*$_2$), 31.99 (*C*H$_2$CH$_2$COOH), 36.67 (CH$_2$*C*H$_2$COOH), 36.70 (*C*HMe$_2$), 62.54 (C(5")), 101.06 (C(3a")), 113.02 (d, ^2J(C, F) = 22.5 Hz; C(6')), 115.39 (d, ^2J(C, F) = 23.2 Hz; C(4')), 121.87 (CN), 124.09 (d, ^4J(C, F) = 2.4 Hz; C(2')), 126.04 (C(4)), 128.14 (C(2)), 129.01 (C(6)), 130.14 (C(5)), 137.65 (C(3")), 141.59 (d, ^4J(C, F) = 2.3 Hz; C(1)), 143.04 (C(3)), 144.52 (d, ^3J(C, F) = 8.1 Hz; C(1')), 148.64 (d, ^3J(C, F) = 6.9 Hz; C(3')), 157.46 (C(7a")), 163.84 (C(6")), 164.57 (d, ^1J(C, F) = 243.7 Hz; C(5')), 176.68 ppm (C=O), C(4") hidden under the residual solvent peak; ^{19}F NMR (377 MHz, CD_3OD): δ = –115.11 ppm (t, ^3J(H, F) = 10.1 Hz; F); IR (ATR): $\tilde{\nu}$ = 3312 (w), 2968 (w), 2188 (m), 1708 (m), 1632 (s), 1582 (s), 1487 (m), 1436 (w), 1385 (s), 1315 (w), 1163 (w), 1042 (w), 941 (w), 864 (w), 827 (w), 792 (w), 701 (s), 633 cm^{-1} (w); HR-ESI-MS: *m/z* (%): 461.1978 (100, $[M + H]^+$, calcd for $C_{26}H_{26}FN_4O_3^+$: 461.1983); analyt. HPLC: t_R = 13.33 min (purity = 98%; method A).

(±)-(1-{3-[6-Amino-5-cyano-3-methyl-4-isopropyl-2,4-dihydropyrano[2,3-*c*]pyrazol-4-yl]-5-fluorophenyl}piperidin-4-yl)acetic Acid ((±)-86). Following general procedure **GP2** (starting from (±)-**95** (148 mg, 0.27 mmol) dissolved in a MeOH (3.40 mL)/THF (1.20 mL) mixture), (±)-**86** (123 mg, 100%) was obtained as a white solid. R_f = 0.17 (SiO_2; cyclohexane/EtOAc/Formic acid 40:60:01); m.p. 153–155 °C; ^{1}H NMR (400 MHz, CD_3OD): δ = 0.86 and 0.98 (d, J = 6.6 Hz, 6 H; CH*Me*$_2$), 1.38 (qt, J = 9.7, 3.5 Hz, 2 H; H$_{ax}$–C(3, 5)), 1.75–1.87 (m, 5 H; H$_{eq}$–C(3, 5) and Me), 1.87–1.98 (m, 1 H; H–C(4)), 2.25 (d, J = 6.9 Hz, 2 H; C*H*$_2$COOH), 2.66–2.79 (m, 3 H; H$_{ax}$–C(2, 6) and C*H*Me$_2$), 3.62 (dt, J = 12.6, 3.4 Hz, 2 H; H$_{eq}$–C(2, 6)), 6.50–6.60 (m, 2 H; H–C(4', 6')), 6.77 ppm (br. t, J = 1.9 Hz, 1 H; H–C(2')); ^{13}C NMR (101 MHz, CD_3OD): δ = 11.95 (Me), 18.93 and 19.37 (CH*Me*$_2$), 32.71 (C(3, 5)), 34.11 (C(4)), 36.65 (*C*HMe$_2$), 41.86 (*C*H$_2$COOH), 50.85 and 50.90 (C(2, 6)), 62.76 (C(5")), 101.37 (C(3a")), 102.58 (d, ^2J(C, F) =

25.4 Hz; C(6')), 107.20 (d, ^{2}J(C, F) = 23.6 Hz; C(4')), 114.16 (d, ^{4}J(C, F) = 2.1 Hz; C(2')), 121.90 (CN), 137.64 (C(3")), 148.12 (d, ^{3}J(C, F) = 8.3 Hz; C(3')), 154.48 (d, ^{3}J(C, F) = 10.3 Hz; C(1')), 157.43 (C(7a")), 163.72 (C(6")), 165.02 (d, ^{1}J(C, F) = 240.7 Hz; C(5')), 176.40 ppm (C=O), C(4") hidden under the residual solvent peak; ^{19}F NMR (377 MHz, CD_3OD): δ = –114.82 ppm (m; F); IR (ATR): $\tilde{\nu}$ = 3311 (w), 2928 (w); 2187 (m), 1707 (m), 1632 (m), 1611 (w), 1583 (s), 1485 (m), 1442 (w), 1382 (s), 1247 (w), 1159 (m), 1107 (w), 1040 (w), 974 (w), 941 (w), 835 (m), 790 (w), 742 (w), 697 cm^{-1} (m); HR-ESI-MS: *m/z* (%): 454.2243 (100, $[M + H]^+$, calcd for $C_{24}H_{29}FN_5O_3^+$: 454.2249); analyt. HPLC: t_R = 7.68 min (purity = 97%; method A).

(+)-(1-{3-[6-Amino-5-cyano-3-methyl-4-isopropyl-2,4-dihydropyrano[2,3-*c*]pyrazol-4-yl]-5-fluorophenyl}piperidin-4-yl)acetic Acid ((+)-86). Following general procedure **GP2** starting from (+)-**95**, (+)-**86** (129 mg, 94%) was obtained as a white solid. ^{1}H NMR (400 MHz, CD_3OD): δ = 0.87 and 0.99 (d, *J* = 6.6 Hz, 6 H; CH*Me*$_2$), 1.38 (qt, *J* = 9.4, 3.6 Hz, 2 H; H_{ax}–C(3, 5)), 1.71–2.00 (m, 6 H; H_{eq}–C(3, 5), H–C(4) and Me), 2.25 (d, *J* = 6.9 Hz, 2 H; C*H*$_2$COOH), 2.59–2.87 (m, 3 H; H_{ax}–C(2, 6) and C*H*Me$_2$), 3.63 (dt, *J* = 12.8, 3.3 Hz, 2 H; H_{eq}–C(2, 6)), 6.50–6.60 (m, 2 H; H–C(4', 6')), 6.78 ppm (t, *J* = 1.9 Hz, 1 H; H–C(2')); (+)-**86**: $[\alpha]^{23}_D$ = 86.4° (*c* 0.50, MeOH).

(–)-(1-{3-[6-Amino-5-cyano-3-methyl-4-isopropyl-2,4-dihydropyrano[2,3-*c*]pyrazol-4-yl]-5-fluorophenyl}piperidin-4-yl)acetic Acid ((–)-86). Following general procedure **GP2** starting from (–)-**95**, (–)-**86** (133 mg, 94%) was obtained as a white solid. ^{1}H NMR (400 MHz, CD_3OD): δ = 0.87 and 0.99 (d, *J* = 6.6 Hz, 6 H; CH*Me*$_2$), 1.38 (qt, *J* = 12.7, 6.0 Hz, 2 H; H_{ax}–C(3, 5)), 1.70–1.98 (m, 6 H; H_{eq}–C(3, 5), H–C(4) and Me), 2.25 (d, *J* = 6.9 Hz, 2 H; C*H*$_2$COOH), 2.69–2.77 (m, 3 H; H_{ax}–C(2, 6) and C*H*Me$_2$), 3.63 (dt, *J* = 12.7, 3.4 Hz, 2 H; H_{eq}–C(2, 6)), 6.50–6.60 (m, 2 H; H–C(4', 6')), 6.77 ppm (d, *J* = 2.0 Hz, 1 H; H–C(2')); (−)-**86**: $[\alpha]^{23}_D$ = −88.0° (*c* 0.50, MeOH).

(±)-3-(1-{3-[6-Amino-5-cyano-3-methyl-4-isopropyl-2,4-dihydropyrano[2,3-*c*]pyrazol-4-yl]-5-fluorophenyl}piperidin-4-yl)propanoic Acid ((±)-87). Following general procedure **GP2**, (±)-**87** (255 mg, 98%) was obtained as a white solid. R_f = 0.18 (SiO_2; cyclohexane/EtOAc/Formic acid 40:60:01); m.p. 153–155 °C; ^{1}H NMR (400 MHz, CD_3OD): δ = 0.87 and 0.99 (d, J = 6.6 Hz, 6 H; CH*Me*$_2$), 1.31 (qt, J = 12.0, 3.7 Hz, 2 H; H_{ax}–C(3, 5)), 1.36–1.50 (m, 1 H; H–C(4)), 1.59 (dt, J = 8.4, 7.0 Hz, 2 H; C*H*$_2$CH$_2$COOH), 1.80 (ddt, J = 11.8, 3.6, 1.9 Hz, 2 H; ; H_{eq}–C(3, 5)), 1.86 (s, 3 H; Me), 2.34 (t, J = 7.6 Hz, 2 H; CH$_2$C*H*$_2$COOH), 2.60–2.82 (m, 3 H; H_{ax}–C(2, 6) and C*H*Me$_2$), 3.63 (dtt, J = 11.9, 4.4, 2.3 Hz, 2 H; H_{eq}–C(2, 6)), 6.52–6.59 (m, 2 H; H–C(4', 6')), 6.77 ppm (br. t, J = 1.9 Hz, 1 H; H–C(2')); ^{13}C NMR (101 MHz, CD_3OD): δ = 11.95 (Me), 18.93 and 19.38 (CH*Me*$_2$), 32.33 (CH$_2$*C*H$_2$COOH), 32.69 (*C*H$_2$CH$_2$COOH), 32.78 (C(3, 5)), 36.52 (C(4)), 36.65 (*C*HMe$_2$), 51.01 and 51.07 (C(2, 6)), 62.77 (C(5")), 101.38 (C(3a")), 102.55 (d, ^2J(C, F) = 25.4 Hz; C(4')), 107.13 (d, ^2J(C, F) = 23.6 Hz; C(6')), 114.17 (d, ^4J(C, F) = 2.1 Hz; C(2')), 121.89 (CN), 137.64 (C(3")), 148.10 (d, ^3J(C, F) = 8.3 Hz; C(3')), 154.54 (d, ^3J(C, F) = 10.3 Hz; C(1')), 157.42 (C(7a")), 163.71 (C(6")), 165.01 (d, ^1J(C, F) = 240.6 Hz; C(5')), 177.70 ppm (C=O), C(4") hidden under the residual solvent peak; ^{19}F NMR (377 MHz, CD_3OD): δ = –114.85 ppm (t, ^3J(H, F) = 11.1 Hz; F); IR (ATR): $\tilde{\nu}$ = 3312 (br. m), 2926 (w), 2188 (m), 1708 (m), 1633 (s), 1583 (s), 1485 (m), 1439 (m), 1381 (s), 1244 (w), 1158 (m), 1108 (w), 1041 (w), 971 (w), 941 (w), 831 (m), 742 (w), 697 cm^{-1} (w); HR-ESI-MS: *m/z* (%): 468.2407 (100, $[M + H]^+$, calcd for $C_{25}H_{31}FN_5O_3^+$: 468.2405); analyt. HPLC: t_R = 8.89 min (purity = 98%; method A).

Benzyl (Piperidin-4-yl)acetate (90). A solution of *tert*-butyl 4-(2-(benzyloxy)-2-oxoethyl)piperidine-1-carboxylate (**92**) (1.75 g, 5.25 mmol, 1.0 eq.) in CH_2Cl_2 (2.40 mL) was cooled down in an ice bath, treated dropwise with TFA (1.20 mL, 15.58 mmol, 3.0 eq.), stirred at

23 °C for 16 h and evaporated. The residue was taken up in EtOAc (30 mL) and sat. K_2CO_3 solution (30 mL). The two layers were separated and the aqueous layer was extracted three times with EtOAc (3 × 20 mL). The combined organic layers were washed with brine, dried over Na_2SO_4, filtered, and evaporated to afford **90** (1.15 g, 94%) as a colorless oil which was directly used for the next step.

***tert*-Butyl 4-[2-(Benzyloxy)-2-oxoethyl]piperidine-1-carboxylate (92).** A solution of 2-(1-(*tert*-butoxycarbonyl)piperidin-4-yl)acetic acid (**91**) (1.35 g, 5.55 mmol, 1.0 eq.) in acetone (20 mL) was treated with K_2CO_3 (0.767 g, 5.55 mmol, 1.0 eq.), followed by benzyl bromide (0.726 mL, 6.10 mmol, 1.1 eq.), stirred at reflux for 16 h, allowed to cool down to 23 °C, and evaporated. The residue was taken up in Et_2O and water. The two layers were separated and the aqueous layer was extracted three times with Et_2O (3 × 20 mL). The combined organic layers were washed with brine, dried over Na_2SO_4, filtered, and evaporated to afford the desired product **92** (1.85 g, 100%) as a colorless oil. R_f = 0.14 (SiO_2; cyclohexane/EtOAc 95:05); ^{1}H NMR (400 MHz, $CDCl_3$): δ = 1.15 (qd, J = 12.4, 4.4 Hz, 2 H; H_{ax}–C(3, 5)), 1.44 (s; C(CH_3)) 1.62–1.75 (m, 2 H; H_{eq}–C(3, 5)), 1.95 (m, 1 H; H–C(4)), 2.29 (d, J = 7.1 Hz, 2 H; CH_2C=O), 2.58–2.86 (m, 2 H; H_{ax}–C(2, 6)), 3.96–4.20 (m, 2 H; H_{eq}–C(2, 6)), 5.12 (s, 2 H; CH_2O), 7.28–7.42 ppm (m, 5 H; H–C(2', 3', 4', 5', 6')); ^{13}C NMR (101 MHz, $CDCl_3$): δ = 28.60 (C(*C*H_3)), 31.94 (C(3, 5)), 33.26 (C(4)), 41.20 (*C*H_2C=O), 43.87 (C(2, 6)), 66.36 (CH_2O), 79.49 (*C*(CH_3)), 128.35 (C(2', 6')), 128.41 (C(4')), 128.72 (C(3', 5')), 136.06 (C(1')), 154.93 (*C*O*t*Bu), 172.37 ppm (*C*OOBn); IR (ATR): $\tilde{\nu}$ = 2975 (w), 2929 (w), 2119 (w), 1733 (m), 1686 (s), 1448 (w), 1419 (m), 1391 (w), 1365 (m), 1313 (w), 1285 (m), 1232 (m), 1151 (s), 1117 (m), 1003 (m), 979 (m), 948 (w), 864 (m), 737 (m), 696 cm^{-1} (s); HR-EI-MS: *m/z* (%): 276.1229 (100, [M – C_4H_9]$^+$, calcd for $C_{15}H_{18}NO_4^+$: 276.1231).

Benzyl {1-[3-Fluoro-5-(2-methylpropanoyl)phenyl]piperidin-4-yl}acetate (93). Dried solvent was used, and the reaction was performed under Argon atmosphere. To a solution of 1-(3-bromo-5-fluorophenyl)-2-methylpropan-1-one (**38**) (4.0 g, 16.32 mmol, 1.0 eq.) in 1,4-dioxane (48 mL) was added benzyl 2-(piperidin-4-yl)acetate (**90**) (4.57 g, 19.58 mmol, 1.2 eq.), followed by Cs_2CO_3 (7.98 g, 24.48 mmol, 1.5 eq.). The mixture was degassed under Ar for 10 min. $[Pd_2(dba)_3]$ (0.299 g, 0.326 mmol, 0.02 eq.) and X-Phos (0.621 g, 1.306 mmol, 0.08 eq.) were added and the mixture was stirred at 110 °C for 10 h. The mixture was allowed to cool down to 25 °C and diluted with EtOAc and water. The aqueous layer was extracted three times with EtOAc (3 × 25 mL). The combined organic layers were washed with brine, dried over Na_2SO_4, filtered, and evaporated. The crude was absorbed on SiO_2 and column chromatography (SiO_2; cyclohexane/EtOAc grad. 100:0 → 90:10) gave **93** (6.1 g, 94%) as a yellow oil. R_f = 0.16 (SiO_2; cyclohexane/EtOAc 90:10); ^{1}H NMR (400 MHz, $CDCl_3$): δ = 1.20 (d, J = 6.8 Hz, 6 H; CHMe_2), 1.39 (dtd, J = 13.2, 11.8, 3.9 Hz, 2 H; H_{ax}–C(3', 5')), 1.76–1.89 (m, 2 H; H_{eq}–C(3', 5')), 2.00 (ttt, J = 10.9, 7.1, 3.7 Hz, 1 H; H–C(4')), 2.34 (d, J = 7.0 Hz, 2 H; CH_2C=O), 2.80 (td, J = 12.4, 2.6 Hz, 2 H; H_{ax}–C(2', 6')), 3.44 (sept., J = 6.8 Hz, 1 H; CHMe$_2$), 3.63–3.79 (m, 2 H; H_{eq}–C(2', 6')), 5.14 (s, 2 H; CH_2O), 6.74 (dt, J = 11.8, 2.3 Hz, 1 H; H–C(4")), 7.01 (ddd, J = 8.9, 2.2, 1.3 Hz, 1 H; H–C(2")), 7.26–7.28 (m, 1 H; H–C(6")), 7.29–7.45 ppm (m, 5 H; H–C(2, 3, 4, 5, 6)); ^{13}C NMR (101 MHz, $CDCl_3$): δ = 19.29 (CHMe_2), 31.61 (C(3', 5')), 32.93 (C(4')), 35.74 (CHMe$_2$), 41.10 (CH$_2$C=O), 49.05 (C(2', 6')), 66.41 (CH_2O), 105.21 (d, ^2J(C, F) = 23.0 Hz; C(2")), 106.84 (d, ^2J(C, F) = 25.3 Hz; C(4")), 111.24 (d, ^4J(C, F) = 2.1 Hz; C(6")), 128.38 (C(2, 6)), 128.44 (C(4)), 128.74 (C(3, 5)), 136.06 (C(1)), 138.58 (d, ^3J(C, F) = 8.0 Hz; C(5")), 153.17 (d, ^3J(C, F) = 9.7 Hz; C(1")), 163.94 (d, ^1J(C, F) = 244.0 Hz; C(3")), 172.35 (OC=O), 203.93 ppm (d, ^4J(C, F) = 2.7 Hz; C=O); ^{19}F NMR (377 MHz, $CDCl_3$): δ = –111.80 ppm (dd, ^3J(H, F) = 11.8, 8.9 Hz;

F); IR (ATR): $\tilde{\nu}$ = 2971 (w), 2932 (w), 1731 (s), 1684 (s), 1606 (s), 1583 (s), 1443 (m), 1383 (m), 1288 (m), 1248 (w), 1149 (s), 1089 (w), 994 (m), 976 (m), 904 (w), 852 (m), 779 (w), 748 (s), 696 (s), 675 cm^{-1} (w); HR-ESI-MS: *m/z* (%): 398.2124 (100, $[M + H]^+$, calcd for $C_{24}H_{29}FNO_3^+$: 398.2126).

Benzyl {1-[3-(1,1-Dicyano-3-methylbut-1-en-2-yl)-5-fluorophenyl]piperidin-4-yl}acetate (94). HPLC grade chloroform distilled over $CaCl_2$ and dried over molecular sieves was used. The reaction was performed under N_2 atmosphere. Benzyl 2-(1-(3-fluoro-5-isobutyrylphenyl)piperidin-4-yl)acetate (**93**) (5.80 g, 14.59 mmol, 1.0 eq.) and malononitrile (4.82 g, 73.0 mmol, 5.0 eq.) were treated with $CHCl_3$ (44 mL). An emulsion was obtained. A dropwise addition of a freshly prepared solution of $TiCl_4$ (2.092 ml, 18.97 mmol, 1.3 eq.) in dry toluene (19 mL) led to a yellow/brown precipitate. Pyridine (4.72 ml, 58.4 mmol, 4.0 eq.) was added, and a black mixture was obtained. The mixture was stirred at 63 °C for 60 h. Addition of 1 M HCl (10 mL) led to a brown precipitate. The mixture was diluted with CH_2Cl_2 (30 mL) and water (30 mL). The layers were separated, and the aqueous layer was filtered to get rid of the precipitate. The aqueous layer was extracted three times with CH_2Cl_2 (3 × 25 mL). The combined organic layers were washed with brine, dried over Na_2SO_4, filtered, and evaporated. The crude was absorbed on SiO_2 and column chromatography (SiO_2; cyclohexane/EtOAc grad. 100:0 → 90:10) gave **94** (5.0 g, 77%) as an orange oil. R_f = 0.29 (SiO_2; cyclohexane/EtOAc 80:20); ^{1}H NMR (400 MHz, $CDCl_3$): δ = 1.20 (d, *J* = 6.9 Hz, 6 H; CH*Me*$_2$), 1.31–1.47 (m, 2 H; H_{ax}–C(3', 5')), 1.78–1.89 (m, 2 H; H_{eq}–C(3', 5')), 2.01 (ddt, *J* = 18.7, 11.2, 4.1 Hz, 1 H; H–C(4')), 2.34 (d, *J* = 7.0 Hz, 2 H; C*H*$_2$C=O), 2.82 (td, *J* = 12.5, 2.7 Hz, 2 H; H_{ax}–C(2', 6')), 3.41 (sept., *J* = 6.9 Hz, 1 H; C*H*Me$_2$), 3.65 (dq, *J* = 12.7, 2.2, 1.6 Hz, 2 H; H_{eq}–C(2', 6')), 5.14 (s, 2 H; CH_2O), 6.28 (ddd, ^3J(H, F) = 8.3 Hz, *J* = 2.2, 1.4 Hz, 1 H; H–C(4")), 6.38 (dd, *J* = 2.4, 1.4 Hz, 1

H; H–C(2")), 6.64 (dt, ^{3}J(H, F) = 12.2 Hz, J = 2.3 Hz, 1 H; H–C(6")), 7.28–7.46 ppm (m, 5 H; H–C(2, 3, 4, 5, 6)); ^{13}C NMR (101 MHz, $CDCl_3$): δ = 20.78 (CHMe_2), 31.48 (C(3', 5')), 32.84 (C(4')), 36.30 (CHMe$_2$), 41.02 (CH$_2$C=O), 48.77 (C(2', 6')), 66.43 (CH$_2$O), 87.08 (C(CN)$_2$), 103.50 (d, ^{2}J(C, F) = 24.4 Hz; C(4")), 104.14 (d, ^{2}J(C, F) = 25.1 Hz; C(6")), 110.01 (d, ^{4}J(C, F) = 2.4 Hz; C(2")), 111.72 (CN), 111.99 (CN), 128.38 (C(2, 6)), 128.45 (C(4)), 128.74(C(3, 5)), 135.91 (d, ^{3}J(C, F) = 10.4 Hz; C(3")), 136.03 (C(1)), 153.19 (d, ^{3}J(C, F) = 10.7 Hz; C(1")), 163.72 (d, ^{1}J(C, F) = 245.6 Hz; C(5")), 172.29 (C=O), 186.23 (d, ^{4}J(C, F) = 2.6 Hz; C=C(CN)$_2$); ^{19}F NMR (377 MHz, $CDCl_3$): δ = –110.29 ppm (dd, J = 12.4, 8.4 Hz; F); IR (ATR): $\tilde{\nu}$ = 2933 (w), 2231 (w), 1730 (s), 1608 (m), 1574 (s), 1462 (m), 1385 (m), 1280 (w), 1240 (w), 1145 (s), 1110 (w), 1093 (w), 1058 (w), 977 (m), 832 (m), 747 (m), 696 (s), 631 cm^{-1} (w); HR-ESI-MS: *m/z* (%): 446.2236 (100, $[M + H]^+$, calcd for $C_{27}H_{29}FN_3O_2^+$: 446.2238).

(±)-Benzyl (1-{3-[6-Amino-5-cyano-3-methyl-4-isopropyl-2,4-dihydropyrano[2,3-*c*]pyrazol-4-yl]-5-fluorophenyl}piperidin-4-yl)acetate ((±)-95). Following general procedure **GP1**, column chromatography (SiO_2; cyclohexane/EtOAc 80:20 → 55:45) and recrystallization from CH_2Cl_2/hexane gave (±)-**95** (145 mg, 25%) as a white solid. R_f = 0.23 (SiO_2; cyclohexane/EtOAc 50:50); m.p. 198–201 °C; ^{1}H NMR (400 MHz, THF-d_8): δ = 0.85 and 0.94 (d, J = 6.6 Hz, 6 H; CHMe_2), 1.35 (qd, J = 12.1, 4.0 Hz, 2 H; H$_{ax}$–C(3', 5')), 1.74–1.82 (m, 2 H; H$_{eq}$–C(3', 5')), 1.87 (s, 4 H; H–C(4') and Me), 2.29 (d, J = 7.0 Hz, 2 H; CH_2C=O), 2.61–2.84 (m, 3 H; H$_{ax}$–C(2', 6') and CHMe$_2$), 3.59–3.70 (m, 2 H; H$_{eq}$–C(2', 6')), 5.08 (s, 2 H; CH$_2$O), 6.04 (br. s, 2 H; NH$_2$), 6.47 (m, 2 H; H–C(4", 6")), 6.78 (t, J = 1.9 Hz, 1 H; H–C(2")), 7.18–7.50 (m, 5 H; H–C(2, 3, 4, 5, 6)), 11.18 ppm (br. s, 1 H; NH); ^{13}C NMR (101 MHz, THF-d_8): δ = 12.31 (Me), 18.95 and 19.42 (CHMe_2), 32.58 (C(3', 5')), 33.91 (C(4')), 36.31 (CHMe$_2$), 41.41 (CH$_2$C=O), 48.69 (d, J = 2.1 Hz; C(4*)), 50.10 and 50.29 (C(2', 6')), 63.77 (C(5*)), 66.36 (CH$_2$O), 100.35 (C(3a*)),

101.66 (d, ^{2}J(C, F) = 25.3 Hz; C(4")), 106.51 (d, ^{2}J(C, F) = 23.3 Hz; C(6")), 113.23 (d, ^{4}J(C, F) = 2.1 Hz; C(2")), 120.16 (CN), 128.66 (C(4)), 128.87 (C(1, 6)), 129.12 (C(3, 5)), 135.71 (C(3*)), 137.72 (C(1)), 147.95 (d, ^{3}J(C, F) = 8.2 Hz; C(3")), 153.93 (d, ^{3}J(C, F) = 10.4 Hz; C(1")), 157.35 (C(7a*)), 162.33 (C(6*)), 164.62 (d, ^{1}J(C, F) = 239.9 Hz; C(5")), 172.20 ppm (C=O); ^{19}F NMR (377 MHz, THF-d_8): δ = –114.59 ppm (m; F); IR (ATR): $\tilde{\nu}$ = 3416 (w), 3228 (w), 3153 (w), 2965 (w), 2195 (s), 1714 (s), 1636 (m), 1612 (w), 1584 (s), 1484 (m), 1462 (w), 1398 (s), 1376 (m), 1347 (w), 1302 (w), 1257 (s), 1174 (m), 1144 (w), 1104 (w), 1075 (w), 1058 (w), 1003 (m), 958 (w), 944 (w), 904 (w), 838 (w), 823 (w), 742 (s), 698 (s), 618 cm^{-1} (w); HR-ESI-MS: *m/z* (%): 544.2719 (100, $[M + H]^+$, calcd for $C_{31}H_{35}FN_5O_3^+$: 544.2718).

Separation of (±)-**95** enantiomers by chiral-phase HPLC (column, Daicel, Chiralpak-IA 250 mm × 20 mm; flow, 15 mL/min; detection, 254 nm; eluent, hexane/EtOAc/*i*PrOH 60:30:10). The sample was dissolved in eluent (7 mg/mL) and injected. (−)-**95**: t_R = 8.41 min (ee > 99%), $[\alpha]^{22}_D$ = −100.6° (*c* 0.51, $CHCl_3$). (+)-**95**: t_R = 9.42 min (ee > 99%), $[\alpha]^{22}_D$ = 103.9° (*c* 0.51, $CHCl_3$); for the HPLC traces see SI, Section S1.10, Figures S1, S2, and S3.

In Vitro Antimalarial Activity. *Plasmodium falciparum* drug-sensitive NF54 strain was cultivated in a variation of the medium previously described, consisting of RPMI 1640 supplemented with 0.5% ALBUMAX® II, 25 mM Hepes, 25 mM $NaHCO_3$ buffer (pH = 7.3), 0.36 mM hypoxanthine, and 100 µg/mL neomycin.[60,61] Human erythrocytes served as host cells. Cultures were maintained in an atmosphere of 3% O_2, 4% CO_2, and 93% N_2 in modular chambers at 37 °C. Compounds were dissolved in DMSO (10 mg/mL), diluted in hypoxanthine-free culture medium, and titrated in duplicates over a 64-fold range in 96 well plates. Infected erythrocytes (1.25% final hematocrit and 0.3% final parasitemia) were added into the wells. After 48 h incubation, 0.25 μCi of [^{3}H]hypoxanthine was added and plates were incubated for an

additional 24 h. Parasites were harvested onto glass-fiber filters, and radioactivity was counted using a betaplate liquid scintillation counter (Wallac, Zurich). The results were recorded and expressed as a percentage of the untreated controls. Fifty percent inhibitory concentrations (EC_{50}) were estimated by linear interpolation.[62]

Enzymatic *Pf*SHMT-Assay. Assay reactions (200 μL total volume) contained SHMT (~ 0.5 μM), L-serine (2 mM), (6S)-THF (0.4 mM), β-$NADP^+$ (0.25 mM), and the coupling enzyme methylene tetrahydrofolate dehydrogenase (FolD, 5 μM) in 50 mM HEPES pH 7.0 containing 1 mM DTT and 0.5 mM EDTA. Reactions were added 1 μL of inhibitors with various concentrations, and initial rates of the reaction were monitored to measure the amount of non-inhibited enzyme. The inhibitors were dissolved in DMSO, and the control assays without inhibitor but in the presence of 0.5% DMSO (final concentration) were also carried out.

Enzymatic *At*SHMT-Assay. Assay reactions (200 μL total volume) contained SHMT (1 μg), L-serine (20 mM), (6S)-THF (0.3 mM), β-NAD^+ (2 mM) and the coupling enzyme methylene tetrahydrofolate dehydrogenase (FolD, 20 μg) in 50 mM Potassium phosphate buffer pH 7.4, containing 7.5 mM DTT. Reactions were added 10 μL of inhibitors with various concentrations (final concentrations from 1–1000 nM), and initial rates of the reaction were monitored to measure the amount of non-inhibited enzyme. The inhibitors were dissolved in 80% DMSO, and the control assays without inhibitor in the presence of 1% DMSO (final concentration) were also carried out. The accumulation of NADH was followed for 20 minutes at 340 nm using a BioTek Synergy HTX plate reader.

In Vitro Cytotoxicity. Rat skeletal myoblasts cells (L6 cells) in RPMI 1640 medium with 10% FCS and 2 mM L-glutamine were added to each well of a 96-well microtiter plate and incubated at 37 °C under a 5% CO_2 atmosphere for 24 h. Compounds were added directly into the wells,

and subsequently serial drug dilutions were prepared covering a range from 100–0.002 μM. The plates were incubated for another 72 h. 10 μL of Alamar Blue (12.5 mg resazurin dissolved in 100 mL water) were then added to each well and incubation continued for a further 1–4 h. The plates were read with a *Spectramax Gemini XS* microplate fluorometer (*Molecular Devices Cooperation*, Sunnyvale, CA, USA) using an excitation wavelength of 536 nm and an emission wavelength of 588 nm. Data were analyzed using the software *Softmax Pro* (*Molecular Devices Cooperation*, Sunnyvale, CA, USA). Decrease of fluorescence (= inhibition) was expressed as percentage of the fluorescence of control cultures and plotted against the drug concentrations. From the sigmoidal inhibition curves, the IC_{50} values were calculated. Podophyllotoxin was used as positive control in the assay (IC_{50} = 0.0082 μM).

Crystallization of Recombinant *Pv*SHMT and Compounds (±)-4, (±)-7, (±)-80, (±)-81, and (±)-85. *Pv*SHMT was crystallized using microbatch method in a 60-well plate (∅ 1 mm at bottom of each well) covered with 6 mL of baby oil (Johnson; a mixture of mineral oil, olive oil, and vitamin E, PZ Johnson, Thailand). Protein-ligand complexes were prepared by mixing 60 μL of purified *Pv*SHMT protein (20–25 mg/mL) with 1 mM PLP, 60 mM β-mercaptoethanol, 90 mM of glycine, and 3.2 mM (±)-**4**, or (±)-**7**, or (±)-**80**, or (±)-**81**, or (±)-**85**. The mixture was equilibrated on ice for 30 min to allow for complete complex formation. The crystallization drop is composed of 1 μL each of a crystallization solution and the protein complex. Protein crystals of *Pv*SHMT were grown at 293 K in 20–24% w/v PEG4000, 0.06–0.12 M NaCl, 0.1 M Tris-HCl buffer pH 8.5 and additive 10% v/v trifluoroethanol.

***Pv*SHMT Crystal Structure Data Collection, Structure Determination and Refinement.** A single crystal was flash-vitrified in liquid nitrogen using 20% glycerol in crystallizing agent as a cryoprotectant. X-ray diffraction data were collected at 100 K at wavelength of 1 Å using ADSC

Quantum-315 CCD detector at beamline 13B1, NSRRC, Taiwan. Data were processed using HKL2000 package. X-ray diffraction data and refinement statistics are listed in SI, Section S4.3, Table S32. The structure of *Pv*SHMT was determined by molecular replacement using *Phaser* in CCP4 suite with a chain A protomer of *Pv*SHMT coordinate (PDB ID code 4OYT) as the template. Model building and structure refinement were carried out using *Coot* and *Refmac5*. The ligand structure was prepared using *HYPERCHEM*.

ASSOCIATED CONTENT

Supporting Information. Additional figures on protein-ligand interactions and design of ligands by modeling; detailed biological activity; detailed biological methods for metabolic stability, metabolite identification and solubility measurements; mutagenicity and plasma protein assessment; hERG inhibition; synthetic procedures, compound characterization, and NMR spectra; molecular formula strings (CSV). This material is available free of charge via the Internet at http://pubs.acs.org.

AUTHOR INFORMATION

Corresponding Author

*To whom correspondence should be addressed:

Prof. François Diederich, Laboratorium für Organische Chemie, ETH Zurich, Vladimir-Prelog-Weg 3, 8093 Zurich, Switzerland, Phone: (+41) 44 632 29 92, E-mail: diederich@org.chem.ethz.ch.

Author Contributions

GS, MW, MR, RB, UL, PC, PC, and FD designed research; GS, PC, AJ, WI, AS, RA, SC, KW, AK, SS, ML, GF, MS, and AZ performed research; GS, MW, MR, RB, UL, PC, PC, and FD analyzed data; GS, MW, MR, RB, UL, PC, PC, and FD wrote the paper.

Notes

The authors declare no conflict of interest.

ACKNOWLEDGMENT

Work at ETH Zurich was supported by a grant from the ETH Research Council (ETH-01 13-2). At ETH Zurich, we thank Dr. Bruno Bernet for help with the compound characterizations, Dr. Christoph Hohn for proofreading the manuscript, and Dr. Nils Trapp for small molecule crystallography. We are grateful to Marcel Kaiser and his technicians for performing the cytotoxicity assay. We are thankful to Sergio Wittlin, Ursula Lehmann, and Christin Gumpp for *in vivo* SCID mouse testing. We thank the MMV foundation, especially Jeremy Burrows, for their support, for giving us access to their assay network, and their great expertise. Protein-ligand studies including *Plasmodium* enzyme kinetic inhibition and protein crystallography were financially supported by grants from Cluster Program and Management Office, National Science and Technology development Agency, Thailand (CPMO-P-13-00835), National Center for Genetic Engineering and Biotechnology (Platform P-14-50241), Thailand Research Fund (RTA5980001), and Mahidol University. We gratefully acknowledge the National Synchrotron Radiation Research Center (Taiwan) for the beamline 13B1 and the staffs. We thank the

experimental facility and the technical services provided by the "Synchrotron Radiation Protein Crystallography Facility of the National Core Facility Program for Biotechnology, Ministry of Science and Technology" and the "National Synchrotron Radiation Research Center", a national user facility supported by the Ministry of Science and Technology, Taiwan, ROC.

ABBREVIATIONS

ACT, artemisinin-based combination therapy; *At*, *Arabidopsis thaliana*; DHF, dihydrofolate; DHFR, dihydrofolate reductase; DHFS, dihydrofolate synthase; DHP, dihydropteroate; DHPS, dihydropteroate synthase; dba, dibenzylideneacetone; dppf, 1,1'-bis(diphenylphosphino)ferrocene; dTMP, deoxythymidine monophosphate; dUMP, deoxyuridine monophosphate; hERG, human Ether-à-gogo Related Gene; HPLC, High-Performance Liquid Chromatography; DMA, *N*,*N*-Dimethylacetamide; *p*ABA, *para*-aminobenzoic acid; *Pb*, *Plasmodium berghei*; *Pf*, *Plasmodium falciparum*; PLP, pyridoxal 5'-phosphate; *Pv*, *Plasmodium vivax*; SHMT, serine hydroxymethyltransferase; TFA, trifluoroacetic acid; THF, tetrahydrofolate; TS, thymidylate synthase; X-Phos, 2-dicyclohexylphosphino-2',4',6'-triisopropylbiphenyl; 5,10-CH_2-THF, 5,10-methylenetetrahydrofolate; μw, microwave irradiation.

REFERENCES

1. Tu, Y. The discovery of artemisinin (qinghaosu) and gifts from Chinese medicine. *Nat. Med.* **2011**, *17*, 1217–1220.

2. Dondorp, A. M.; Fairhurst, R. M.; Slutsker, L.; MacArthur, J. R.; Breman, J. G.; Guerrin, P. J.; Wellems, T. E.; Ringwald, P.; Newman, R. D.; Plowe, C. V. The threat of artemisinin-resistant malaria. *N. Engl. J. Med.* **2011**, *365*, 1073–1075.

3. Ashley, E. A. and 82 more co-authors from the Tracking Resistance to Artemisinin Collaboration (TRAC), Spread of artemisinin resistance in *Plasmodium falciparum* malaria. *N. Engl. J. Med.* **2014**, *371*, 411–423.

4. World Health Organization. *Artemisinin and artemisinin-based combination therapy resistance. Status Report Global Malaria Programme*; World Health Organization: Geneva October **2016**.

5. Mbengue, A.; Bhattacharjee, S.; Pandharkar, T.; Liu, H.; Estiu, G.; Stahelin, R. V.; Rizk, S. S.; Njimoh, D. L.; Ryan, Y.; Chotivanich, K.; Nguon, C.; Ghorbal, M.; Lopez-Rubio, J.-J.; Pfrender, M.; Emrich, S.; Mohandas, N.; Dondorp, A. M.; Wiest, O.; Haldar, K. A molecular mechanism of artemisinin resistance in *Plasmodium falciparum* malaria. *Nature* **2015**, *520*, 683–687.

6. Burrows, J. Malaria runs rings round artemisinin. *Nature* **2015**, *520*, 628–629.

7. Paloque, L.; Ramadani, A. P.; Mercereau-Puijalon, O.; Augereau, J.-M.; Benoit-Vical, F. *Plasmodium falciparum*: multifaceted resistance to artemisinins. *Malar. J.* **2016**, *15*:149. DOI: 10.1186/s12936-016-1206-9.

8. O'Neill, P. M.; Barton, V. E.; Ward, S. A. The molecular mechanism of action of artemisinin–the debate continues. *Molecules* **2010**, *15*, 1705–1721.

9. Rosenthal, P. J. The interplay between drug resistance and fitness in malaria parasites. *Mol. Microbiol.* **2013**, *89*, 1025–1038.

10. Haynes, R. K.; Fugmann, B.; Stetter, J.; Rieckmann, K.; Heilmann, H.-D.; Chan, H.-W.; Cheung, M.-K.; Lam, W.-L.; Wong, H.-N.; Croft, S. L.; Vivas, L.; Rattray, L.; Stewart, L.; Peters, W.; Robinson, B. L.; Edstein, M. D.; Kotecka, B.; Kyle, D. E.; Beckermann, B.; Gerisch, M.; Radtke, M.; Schmuck, G.; Steinke, W.; Wollborn, U.; Schmeer, K.; Römer, A. Artemisone–a highly active antimalarial drug of the artemisinin class. *Angew. Chem. Int. Ed.* **2006**, *45*, 2082–2088.

11. Charman, S. A.; Arbe-Barnes, S.; Bathurst, I. C.; Brun, R.; Campbell, M.; Charman, W. N.; Chiu, F. C. K.; Chollet, J.; Craft, J. C.; Creek, D. J.; Dong, Y.; Matile, H.; Maurer, M.; Morizzi, J.; Nguyen, T.; Papastogiannidis, P.; Scheurer, C.; Shackleford, D. M.; Sriraghavan, K.; Stingelin, L.; Tang, Y.; Urwyler, H.; Wang, X.; White, K. L.; Wittlin, S.; Zhou, L.; Vennerstrom, J. L. Synthetic ozonide drug candidate OZ439 offers new hope for a single-dose cure of uncomplicated malaria. *Proc. Natl. Acad. Sci. U. S. A.* **2011**, *108*, 4400–4405.

12. Rottmann, M.; McNamara, C.; Yeung, B. K. S.; Lee, M. C. S.; Zou, B.; Russell, B.; Seitz, P.; Plouffe, D. M.; Dharia, N. V.; Tan, J.; Cohen, S. B.; Spencer, K. R.; González-Páez, G. E.; Lakshminarayana, S. B.; Goh, A.; Suwanarusk, R.; Jegla, T.; Schmitt, E. K.; Beck, H.-P.; Brun, R.; Nosten, F.; Renia, L.; Dartois, V.; Keller, T. H.; Fidock, D. A.; Winzeler, E. A.; Diagana, T. T. Spiroindolones, a potent compound class for the treatment of malaria. *Science* **2010**, *329*, 1175–1180.

13. White, N. J.; Pukrittayakamee, S.; Phyo, A. P.; Rueangweerayut, R.; Nosten, F.; Jittamala, P.; Jeeyapant, A.; Jain, J. P.; Lefèvre, G.; Li, R.; Magnusson, B.; Diagana, T. T.;

Leong, F. J. Spiroindolone KAE609 for *falciparum* and *vivax* malaria. *N. Engl. J. Med.* **2014**, *371*, 403–410.

14. Nagle, A.; Wu, T.; Kuhen, K.; Gagaring, K.; Borboa, R.; Francek, C.; Chen, Z.; Plouffe, D.; Lin, X.; Caldwell, C.; Ek, J.; Skolnik, S.; Liu, F.; Wang, J.; Chang, J.; Li, C.; Liu, B.; Hollenbeck, T.; Tuntland, T.; Isbell, J.; Chuan, T.; Alper, P. B.; Fischli, C.; Brun, R.; Lakshminarayana, S. B.; Rottmann, M.; Diagana, T. T.; Winzeler, E. A.; Glynne, R.; Tully, D. C.; Chatterjee, A. K. Imidazolopiperazines: lead optimization of the second-generation antimalarial agents. *J. Med. Chem.* **2012**, *55*, 4244–4273.

15. Kuhen, K. L. and 37 other co-authors. KAF156 is an antimalarial clinical candidate with potential for use in prophylaxis, treatment, and prevention of disease transmission. *Antimicrob. Agents Ch.* **2014**, *58*, 5060–5067.

16. Leong, F. J.; Zhao, R.; Zeng, S.; Magnusson, B.; Diagana, T. T.; Pertel, P. A first-in-human randomized, double-blind, placebo-controlled, single- and multiple-ascending oral dose study of novel imidazolopiperazine KAF156 to assess its safety, tolerability, and pharmacokinetics in healthy adult volunteers. *Antimicrob. Agents Ch.* **2014,** *58*, 6437–6443.

17. White, N. J.; Duong, T. T.; Uthaisin, C.; Nosten, F.; Phyo, A. P.; Hanboonkunupakarn, B.; Pukrittayakamee, S.; Jittamala, P.; Chuthasmit, K.; Cheung, M. S.; Feng, Y.; Li, R.; Magnusson, B.; Sultan, M.; Wieser, D.; Xun, X.; Zhao, R.; Diagana, T. T.; Pertel, P.; Leong, F. J. Antimalarial Activity of KAF156 in Falciparum and Vivax Malaria. *N. Engl. J. Med.* **2016**, *375*, 1152–1160.

18. Baragaña, B. and 62 other co-authors. A novel multiple-stage antimalarial agent that inhibits protein synthesis. *Nature* **2015**, *522*, 315–320.

19. Kato, N. and 51 other co-authors. Diversity-oriented synthesis yields novel multistage antimalarial inhibitors. *Nature* **2016**, *358*, 344–349.

20. Li, H.; O'Donoghue, A. J.; van der Linden, W. A.; Xie, S. C.; Yoo, E.; Foe, I. T.; Tilley, L.; Craik, C. S.; da Fonseca, P. C. A.; Bogyo, M. Structure- and function-based design of *Plasmodium*-selective proteasome inhibitors. *Nature* **2016**, *530*, 233–236.

21. Phillips, M. A. and 53 other co-authors. A long duration dihydroorotate dehydrogenase inhibitor (DSM265) for prevention and treatment of malaria. *Sci. Transl. Med.* **2015**, *7*, 1–12. DOI: 10.1126/scitranslmed.aaa6645.

22. Yuthavong, Y.; Tarnchompoo, B.; Vilaivan, T.; Chitnumsub, P.; Kamchonwongpaisan, S.; Charman, S. A.; McLennan, D. N.; White, K. L.; Vivas, L.; Bongard, E.; Thongpanchang, C.; Taweechai, S.; Vanichtanankul, J.; Rattanajak, R.; Arwon, U.; Fantauzzi, P.; Yuvaniyama, J.; Charman, W. N.; Matthews, D. Malarial dihydrofolate reductase as a paradigm for drug development against a resistance-compromised target. *Proc. Natl. Acad. Sci. U. S. A.* **2012**, *109*, 16823–16828.

23. Nirmalan, N.; Wang, P.; Sims, P. F. G.; Hyde, J. E. Transcriptional analysis of genes encoding enzymes of the folate pathway in the human malaria parasite *Plasmodium falciparum*. *Mol. Microbiol.* **2002**, *46*, 179–190.

24. Szebenyi, D. M. E.; Musayev, F. N.; di Salvo, M. L.; Safo, M. K.; Schirch, V. Serine hydroxymethyltransferase: role of Glu75 and evidence that serine is cleaved by a retroaldol mechanism. *Biochemistry* **2004**, *43*, 6865–6876.

25. Schirch, V.; Szebenyi, D. M. E. Serine hydroxymethyltransferase revisited. *Curr. Opin. Chem. Biol.* **2005**, *9*, 482–487.

26. França, T. C. C.; Pascutti, P. G.; Ramalho, T. C.; Figueroa-Villar, J. D. A three-dimensional structure of *Plasmodium falciparum* serine hydroxymethyltransferase in complex with glycine and 5-formyl-tetrahydrofolate. Homology modeling and molecular dynamics. *Biophys. Chem.* **2005**, *115*, 1–10.

27. França, T. C. C.; Wilter, A.; Ramalho, T. C.; Pascutti, P. G.; Figueroa-Villar, J. D. Molecular dynamics of the interaction of *Plasmodium falciparum* and human serine hydroxymethyltransferase with 5-formyl-6-hydrofolic acid analogues: design of new potential antimalarials. *J. Braz. Chem. Soc.* **2006**, *17*, 1383–1392.

28. Maenpuen, S.; Sopitthummakhun, K.; Yuthavong, Y.; Chaiyen, P.; Leartsakulpanich, U. Characterization of *Plasmodium falciparum* serine hydroxymethyltransferase–A potential antimalarial target. *Mol. Biochem. Parasitol.* **2009**, *168*, 63–73.

29. Pang, C. K. T.; Hunter, J. H.; Gujjar, R.; Podutoori, R.; Bowman, J.; Mudeppa, D. G.; Rathod, P. K. Catalytic and ligand-binding characteristics of *Plasmodium falciparum* serine hydroxymethyltransferase. *Mol. Biochem. Parasitol.* **2009**, *168*, 74–83.

30. Sopitthummakhun, K.; Maenpuen, S.; Yuthavong, Y.; Leartsakulpanich, U.; Chaiyen, P. Serine hydroxymethyltransferase from *Plasmodium vivax* serine is different in substrate specificity from its homologues. *FEBS J.* **2009**, *276*, 4023–4036.

31. da Silva, M. L.; da Silva Gonçalves, A.; Batista, P. R.; Figueroa-Villar, J. D.; Pascutti, P. G.; França, T. C. C. Design, docking studies and molecular dynamics of new potential selective

inhibitors of *Plasmodium falciparum* serine hydroxymethyltransferase. *Mol. Simulat.* **2010**, *36*, 5–14.

32. Read, M.; Müller, I. B.; Mitchell, S. L.; Sims, P. F. G. ; Hyde, J. E. Dynamic subcellular localization of isoforms of the folate pathway enzyme serine hydroxymethyltransferase (SHMT) through the erythrocytic cycle of *Plasmodium falciparum*. *Malaria J.* **2010**, *9*:351.

33. Sopitthummakhun, K.; Thongpanchang, C.; Vilaivan, T.; Yuthavong, Y.; Chaiyen, P.; Leartsakulpanich, U. *Plasmodium* serine hydroxymethyltransferase as a potential anti-malarial target: inhibition studies using improved methods for enzyme production and assay. *Malaria J.* **2012**, *11*:194.

34. Pornthanakasem, W.; Kongkasuriyachai, D.; Uthaipibull, C.; Yuthavong, Y.; Leartsakulpanich, U. *Plasmodium* serine hydroxymethyltransferase: indispensability and display of distinct localization. *Malaria J.* **2012**, *11*:387.

35. Chitnumsub, P.; Ittarat, W.; Jaruwat, A.; Noytanom, K.; Amornwatcharapong, W.; Pornthanakasem, W.; Chaiyen, P.; Yuthavong, Y.; Leartsakulpanich, U. The structure of *Plasmodium falciparum* serine hydroxymethyltransferase reveals a novel redox switch that regulates its activities. *Acta Crystallogr.* **2014**, *D70*, 1517–1527.

36. Chitnumsub, P.; Jaruwat, A.; Riangrungroj, P.; Ittarat, W.; Noytanom, K.; Oonanant, W.; Vanichthanankul, J.; Chuankhayan, P.; Maenpuen, S.; Chen, C.-J.; Chaiyen, P.; Yuthavong, Y.; Leartsakulpanich, U., Structures of *Plasmodium vivax* serine hydroxymethyltransferase: implications for ligand-binding specificity and functional control. *Acta Crystallogr.* **2014**, *D70*, 3177–3186.

37. Wright, D. L.; Anderson, A. C: Antifolate agents: a patent review (2006 – 2010). *Expert Opin. Ther. Patents* **2011**, *21*, 1293–1308.

38. Salcedo-Sora, J. E.; Ward, S. A. The folate metabolic network of *Falciparum* malaria. *Mol. Biochem. Parasitol.* **2013**, *188*, 51–62.

39. Müller, I. B.; Hyde, J. E. Folate metabolism in human malaria parasites–75 years on. *Mol. Biochem. Parasitol.* **2013**, *188*, 63–77.

40. Witschel, M. C.; Rottmann, M.; Schwab, A.; Leartsakulpanich, U.; Chitnumsub, P.; Seet, M.; Tonazzi, S.; Schwertz, G.; Stelzer, F.; Mietzner, T.; McNamara, C.; Thater, F.; Freymond, C.; Jaruwat, A.; Pinthong, C.; Riangrungroj, P.; Oufir, M.; Hamburger, M.; Mäser, P.; Sanz-Alonso, L. M.; Charman, S.; Wittlin, S.; Yuthavong, Y.; Chaiyen, P.; Diederich, F. Inhibitors of plasmodial serine hydroxymethyltransferase (SHMT): cocrystal structures of pyrazolopyrans with potent blood- and liver-stage activities. *J. Med. Chem.* **2015**, *58*, 3117–3130.

41. Marani, M.; Paone, A.; Fiascarelli, A.; Macone, A.; Gargano, M.; Rinaldo, S.; Giardina, G.; Pontecorvi, V.; Koes, D.; McDermott, L.; Yang, T.; Paiardini, A.; Contestabile, R.; Cutruzzolà, F. A pyrazolopyran derivative preferentially inhibits the activity of human cytosolic serine hydroxymethyltransferase and induces cell death in lung cancer cells. *Oncotarget* **2015**, *7*, 4570–4583.

42. Paiardini, A.; Fiascarelli, A.; Rinaldo, S.; Daidone, F.; Giardina, G.; Koes, D. R.; Parroni, A.; Montini, G.; Marani, M.; Paone, A.; McDermott, L. A.; Contestabile, R.; Cutruzzolà, F. Screening and in vitro testing of antifolate inhibitors of human cytosolic serine hydroxymethyltransferase. *ChemMedChem* **2015,** *10*, 490–497.

43. Kim, D.; Fiske, B. P.; Birsoy, K.; Freinkman, E.; Kami, K.; Possemato, R. L.; Chudnovsky, Y.; Pacold, M. E.; Chen, W. W.; Cantor, J. R.; Shelton, L. M.; Gui, D. Y.; Kwon, M.; Ramkissoon, S. H.; Ligon, K. L.; Kang, S. W.; Snuderl, M.; Vander Heiden, M. G.; Sabatini, D. M. SHMT2 drives glioma cell survival in ischaemia but imposes a dependence on glycine clearance. *Nature* **2015**, *520*, 363–367.

44. Gerber, P. R.; Müller, K. MAB, a generally applicable molecular force field for structure modelling in medicinal chemistry. *J. Comput. Aided Mol. Des.* **1995**, *9*, 251–268.

45. Witschel, M.; Stelzer, F.; Hutzler, J.; Qu, T.; Mietzner, T.; Kreuz, K.; Grossmann, K.; Aponte, R.; Höffken, H. W.; Calo, F.; Ehrhardt, T.; Simon, A.; Parra Rapado, L. Pyrazolopyrans having herbicidal and pharmaceutical properties. *WO 2013/182472 A1* **2013**.

46. Kotha, S; Lahiri, K.; Kashinath, D. Recent applications of the Suzuki-Miyaura cross-coupling reaction in organic synthesis. *Tetrahedron* **2002**, *58*, 9633–9695.

47. Beno, B. R.; Yeung, K.-S.; Bartberger, M. D.; Pennington, L. D.; Meanwell, N. A. A survey of the role of noncovalent sulfur interactions in drug design. *J. Med. Chem.* **2015**, *58*, 4383–4438.

48. Lange, A.; Günther, M.; Büttner, F. M.; Zimmermann, M. O.; Heidrich, J.; Hennig, S.; Zahn, S.; Schall, C.; Sievers-Engler, A.; Ansideri, F.; Koch, P.; Laemmerhofer, M.; Stehle, T.; Laufer, S. A.; Boeckler, F. M. Targeting the gatekeeper MET146 of C-Jun N-Terminal Kinase 3 induces a bivalent halogen/chalcogen bond. *J. Am. Chem. Soc.* **2015**, *137*, 14640–14652.

49. Brameld, K. A.; Kuhn, B.; Reuter, D. C.; Stahl, M. Small molecule conformational preferences derived from crystal structure data. A medicinal chemistry focused analysis. *J. Chem. Inf. Model.* **2008**, *48*, 1–24.

50. Muci, A. R.; Buchwald, S. L. Practical palladium catalysts for C-N and C-O bond formation. *Top. Curr. Chem.* **2002**, *219*, 131–209.

51. Haas, D.; Hammann, J. M.; Greiner, R.; Knochel, P. Recent developments in Negishi cross-coupling reactions. *ACS Catal.* **2016**, *6*, 1540–1552.

52. Jiménez-Díaz, M. B.; Mulet, T.; Viera, S.; Gómez, V.; Garuti, H.; Ibáñez, J.; Alvarez-Doval, A.; Shultz, L. D.; Martínez, A.; Gargallo-Viola, D.; Angulo-Barturen, I. Improved murine model of malaria using *Plasmodium falciparum* competent strains and non-myelodepleted NOD-*scid IL2R*γ^{null} mice engrafted with human erythrocytes. *Antimicrob. Agents Chemother.* **2009**, *53*, 4533–4536.

53. Smith, D. A.; Jones, B. C.; Walter, D. K. Design of drugs involving the concepts and theories of drug metabolism and pharmacokinetics. *Med. Res. Rev.* **1996**, *16*, 243–266.

54. Mortelmans, K.; Zeiger, E. The Ames *Salmonella*/microsome mutagenicity assay. *Mutat. Res.* **2000**, *455*, 29–60.

55. Paulini, R.; Müller, K.; Diederich, F. Orthogonal multipolar interactions in structural chemistry and biology. *Angew. Chem. Int. Ed.* **2005**, *44*, 1788–1805.

56. Müller, K.; Faeh, C.; Diederich, F., Fluorine in pharmaceuticals: looking beyond intuition. *Science* **2007**, *317*, 1881–1886.

57. Persch, E.; Dumele, O.; Diederich, F. Molecular recognition in chemical and biological systems. *Angew. Chem. Int. Ed.* **2015**, *54*, 3290–3327.

58. Bauer, M. R.; Jones, R. N.; Baud, M. G. J.; Wilcken, R.; Boeckler, F. M.; Fersht, A. R.; Joerger, A. C.; Spencer, J. Harnessing fluorine-sulfur contacts and multipolar interactions for the design of p53 mutant Y220C rescue drugs. *ACS Chem. Biol.* **2016**, *11*, 2265–2274.

59. Rabinowitz, J. D.; Kim, H.; Ducker, G. S.; Ghergurovich, J. M. SHMT Inhibitors. *WO 2016/145252 A1* **2016**.

60. Dorn, A.; Stofell, R.; Matile, H.; Bubendorf, A.; Ridley, R. G. Malarial haemozoin/β-haematin supports haem polymerization in the absence of protein. *Nature* **1995**, *374*, 269–271.

61. Trager, W.; Jensen, J. B. Human malaria parasites in continuous culture. **1976**, *193*, 673–675.

62. Huber, W.; Koella, J. C. A comparison of three methods of estimating EC_{50} in studies of drug resistance of malaria parasites. *Acta Tropica* **1993**, *55*, 257–261.

Table of Contents and Abstract Graphic

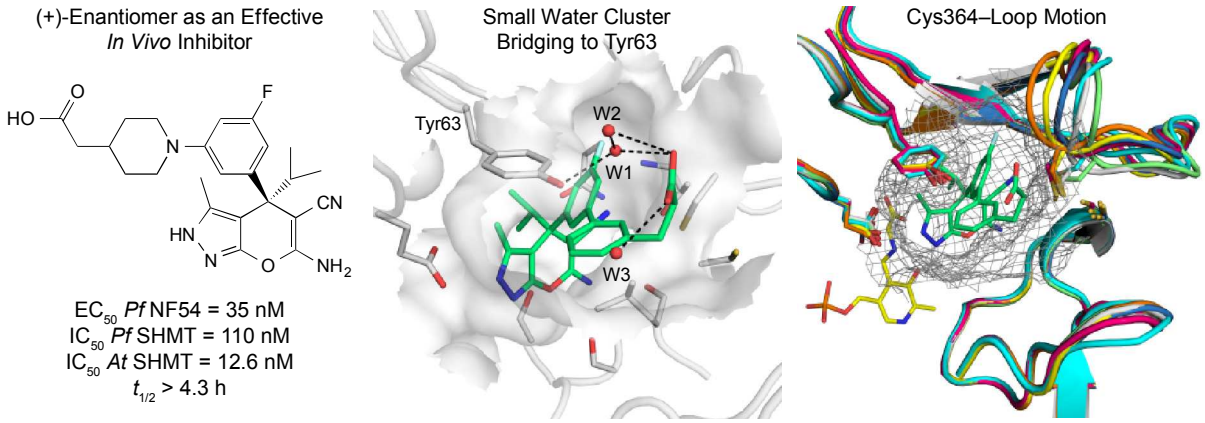

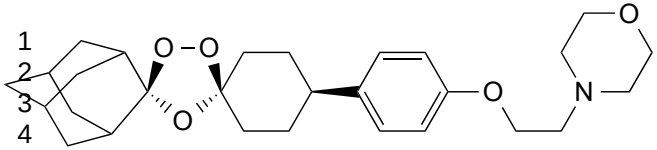

OZ439

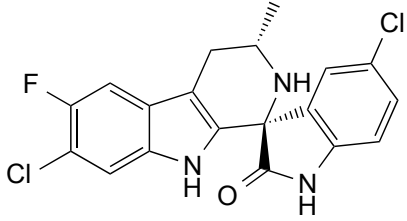

NITD609

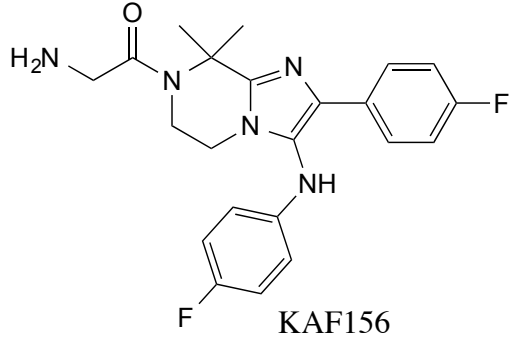

KAF156

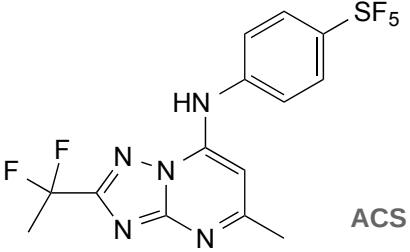

DSM265

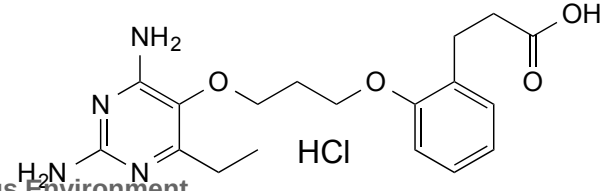

P218

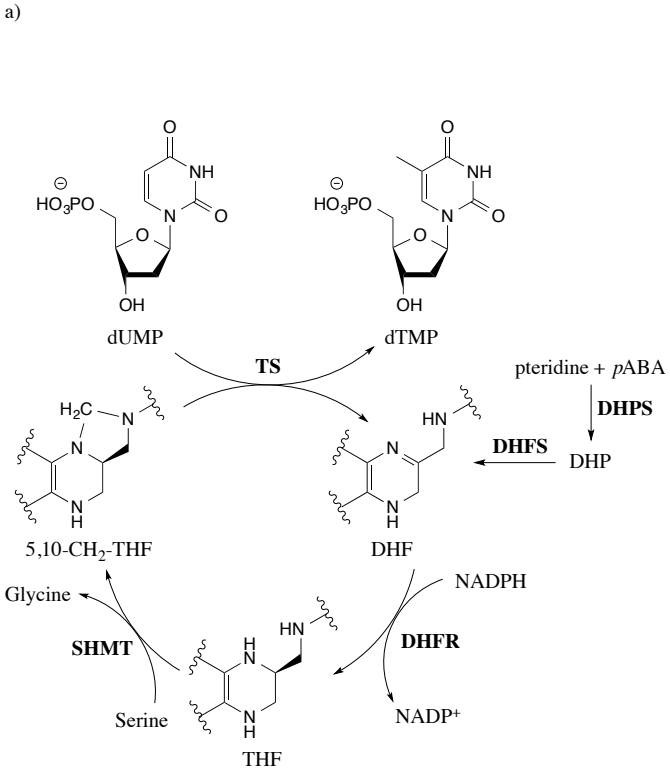

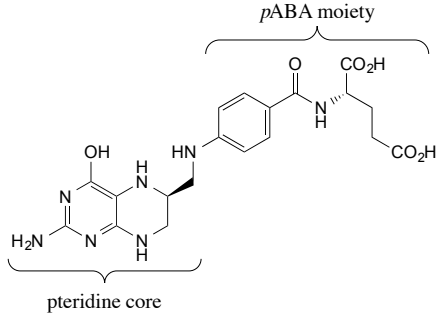

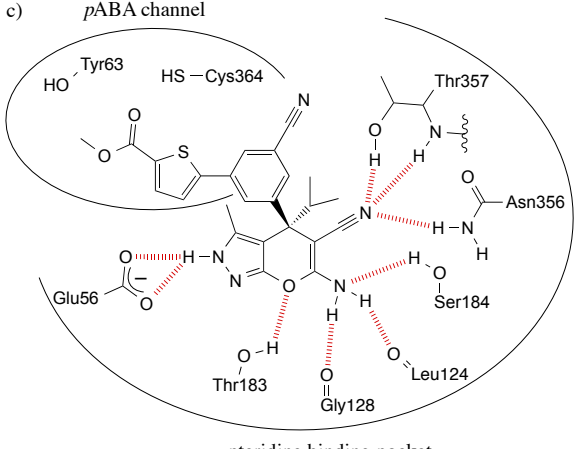

EC_{50} *Pf* NF54: (±)-**1** = 3 nM; (+)-**1** = 2 nM
IC_{50} *Pf* SHMT: (±)-**1** = 370 nM; (+)-**1** = 60 nM

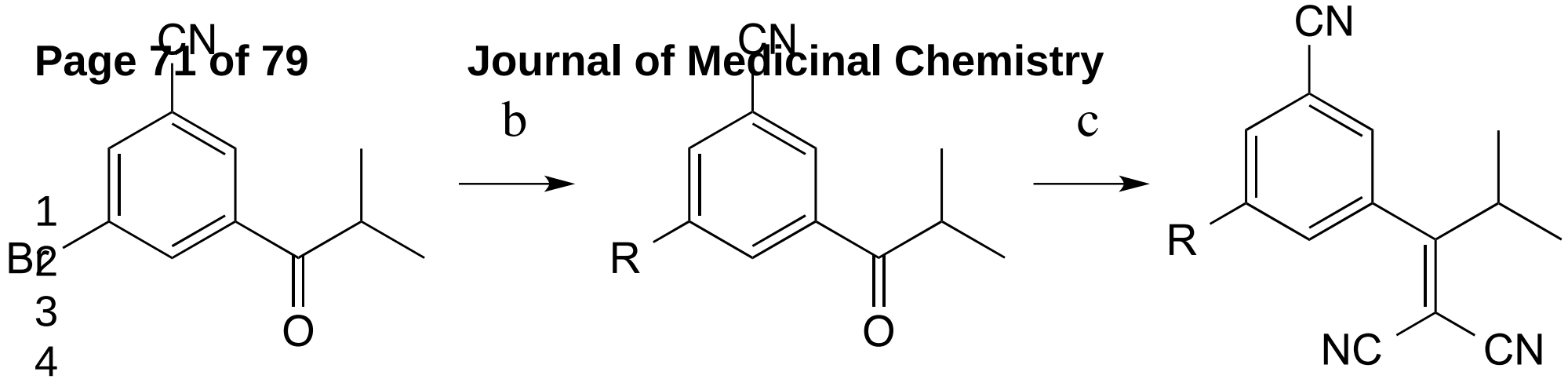

9 → **10** (a)

11a–g

12a–g

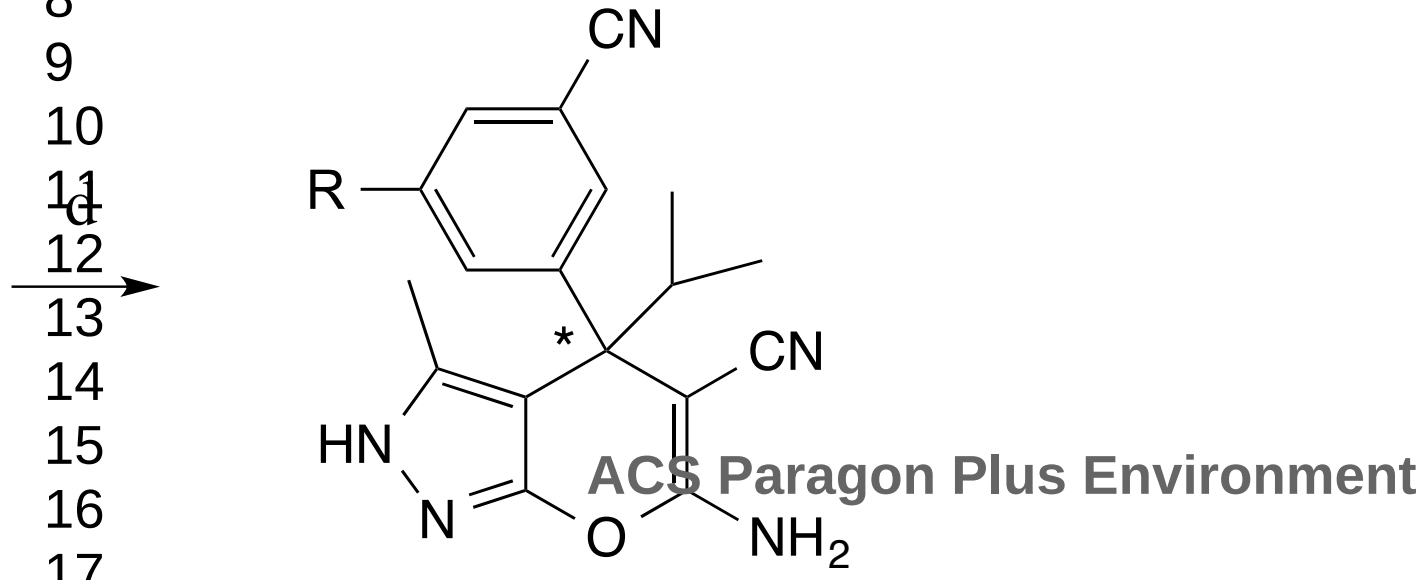

(±)-**2–8**

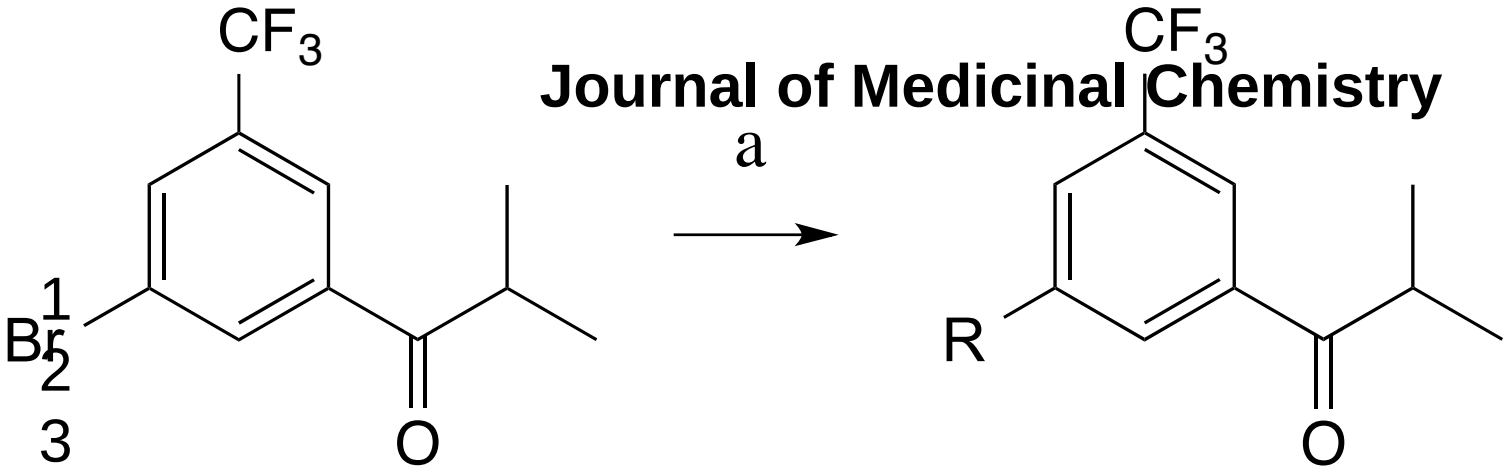

38 **39a–i**

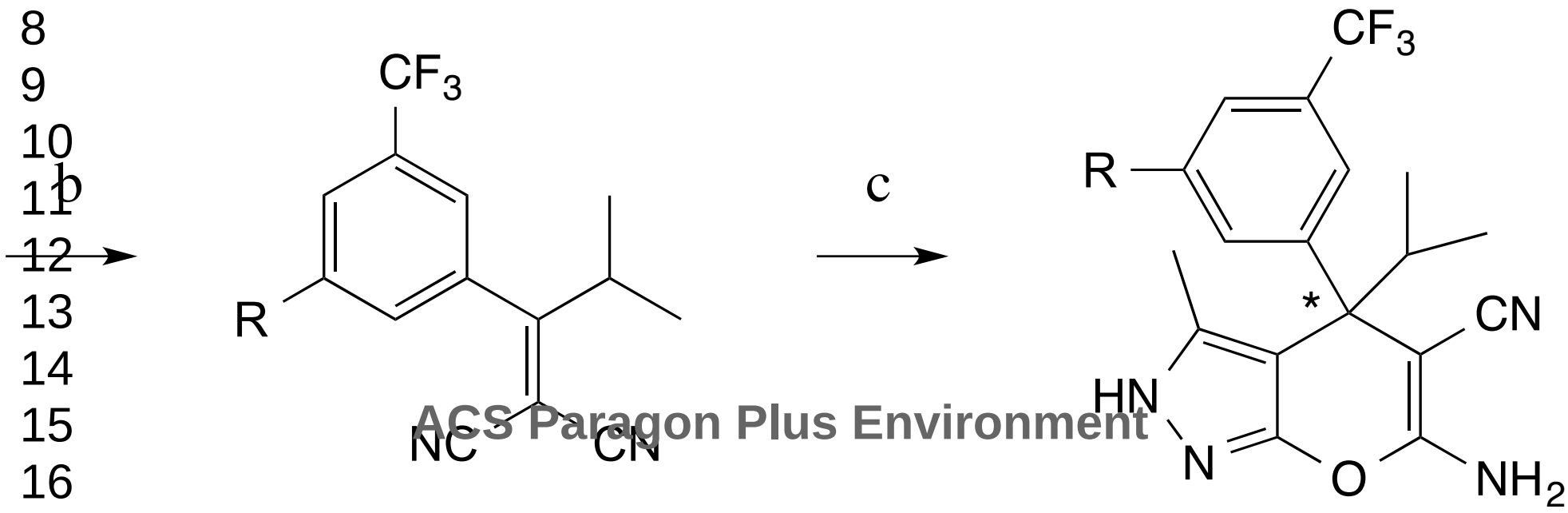

40a–i **(±)-29–37**

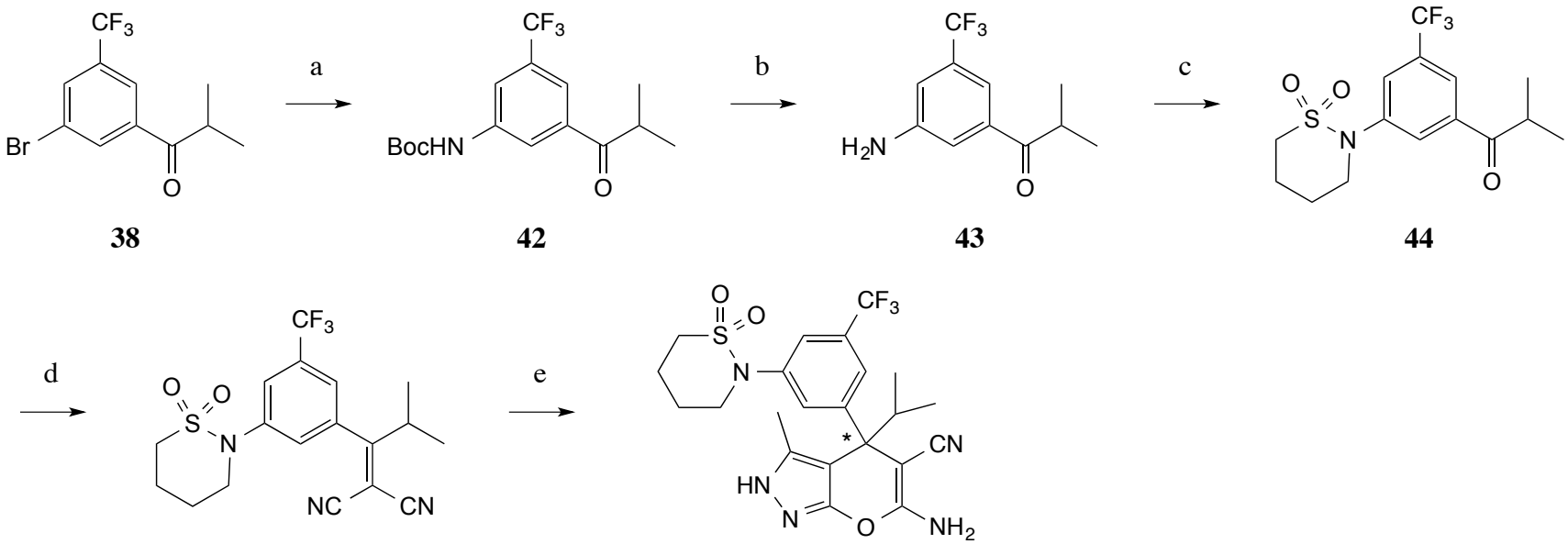

38 **42** **43** **44**

45 (±)-**41**

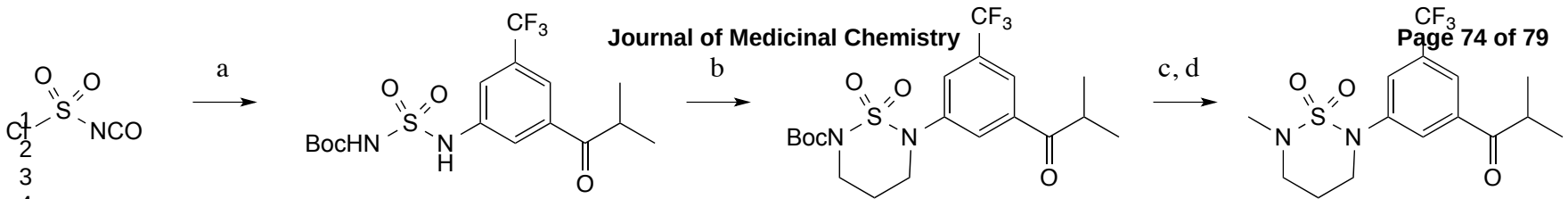

47 **48** **49** **50**

51 (±)-**46**

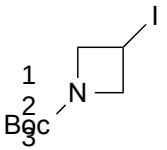

54

a

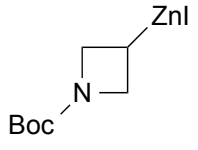

55 (not isolated)

b

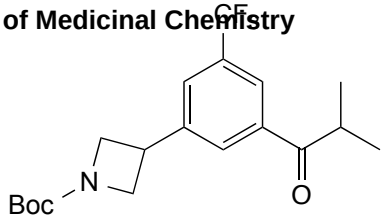

56

c

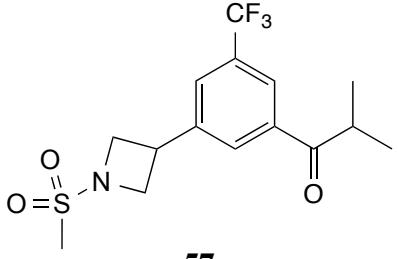

57

d

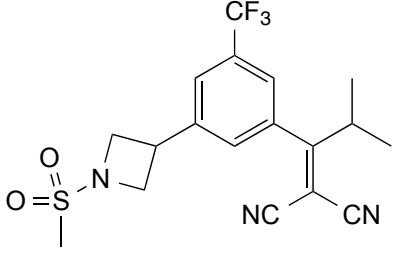

58

e

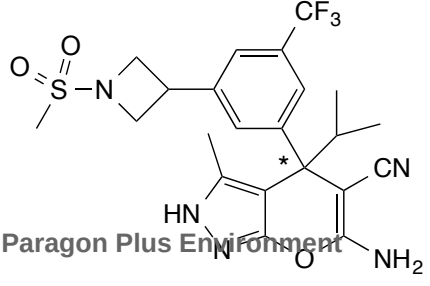

(±)-**53**

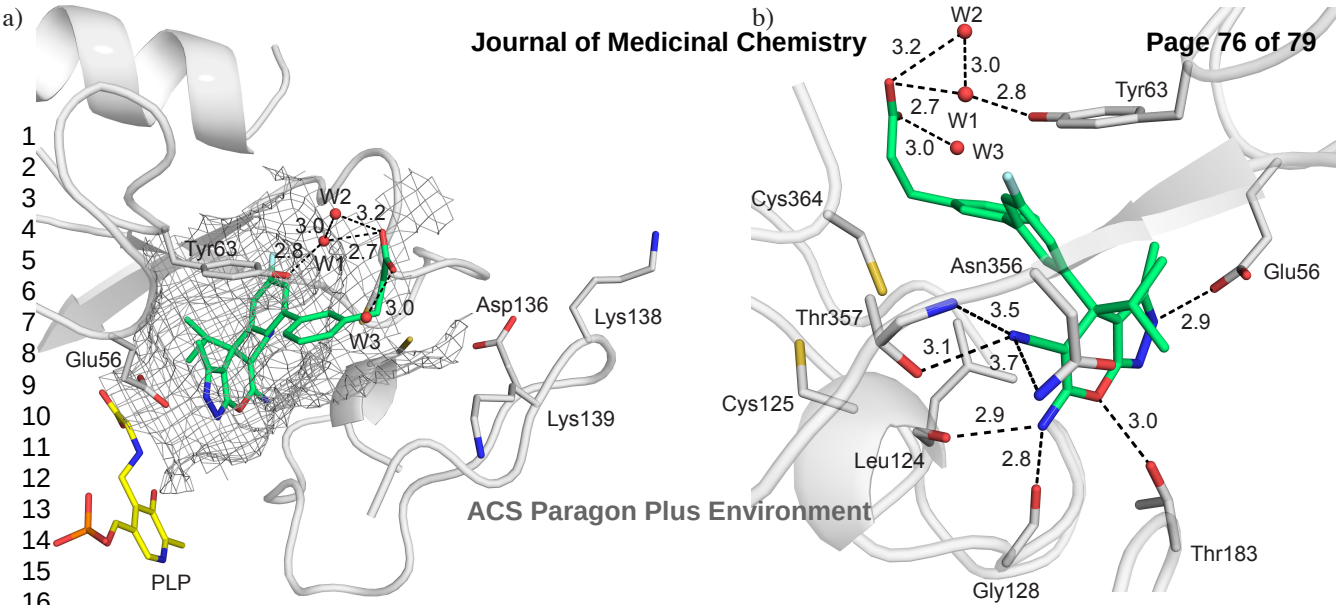
a)
W2
3.2
3.0
2.8
2.7
W1
3.0
W3
Tyr63
Asp136
Lys138
Lys139
Glu56
PLP
b)
W2
3.2
3.0
2.8
2.7
W1
3.0
W3
Tyr63
Cys364
Asn356
Glu56
Thr357
3.5
2.9
3.1
3.7
Cys125
2.9
3.0
Leu124
2.8
Thr183
Gly128
ACS Paragon Plus Environment

a)

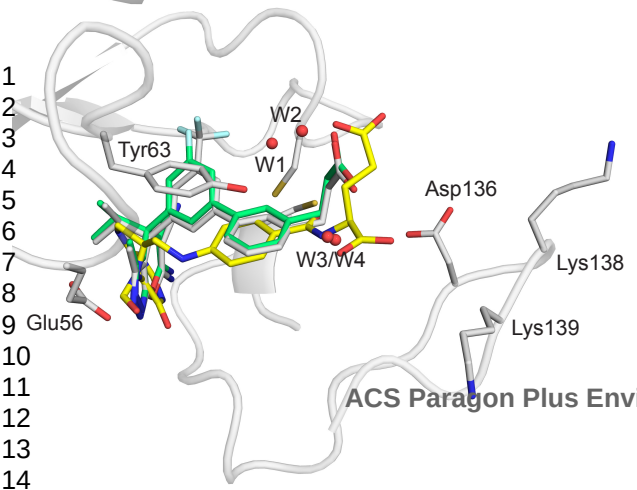

b)

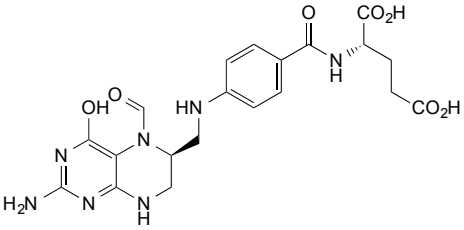

N-formyl-THF

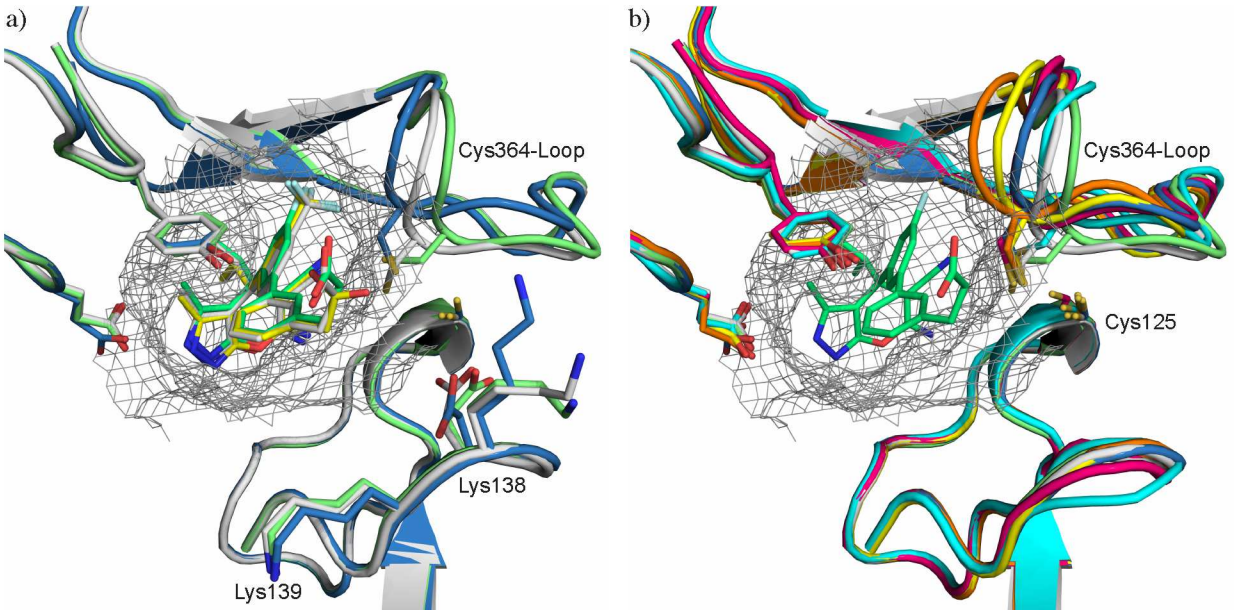
a)
Cys364-Loop
Lys138
Lys139
b)
Cys364-Loop
Cys125

(+)-Enantiomer as an Effective *In Vivo* Inhibitor

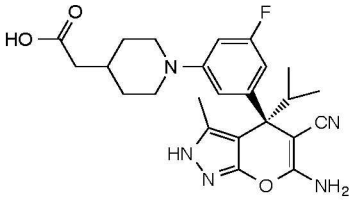

EC_{50} *Pf* NF54 = 35 nM
IC_{50} *Pf* SHMT = 110 nM
IC_{50} *At* SHMT = 12.6 nM
$t_{1/2}$ > 4.3 h

Small Water Cluster Bridging to Tyr63

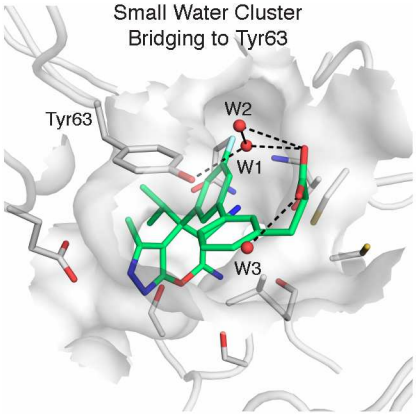

Cys364–Loop Motion